Cell Reports

Article

# Local heterochromatin enrichment promotes telomere clustering and PML nuclear body assembly at telomeres

## Graphical abstract

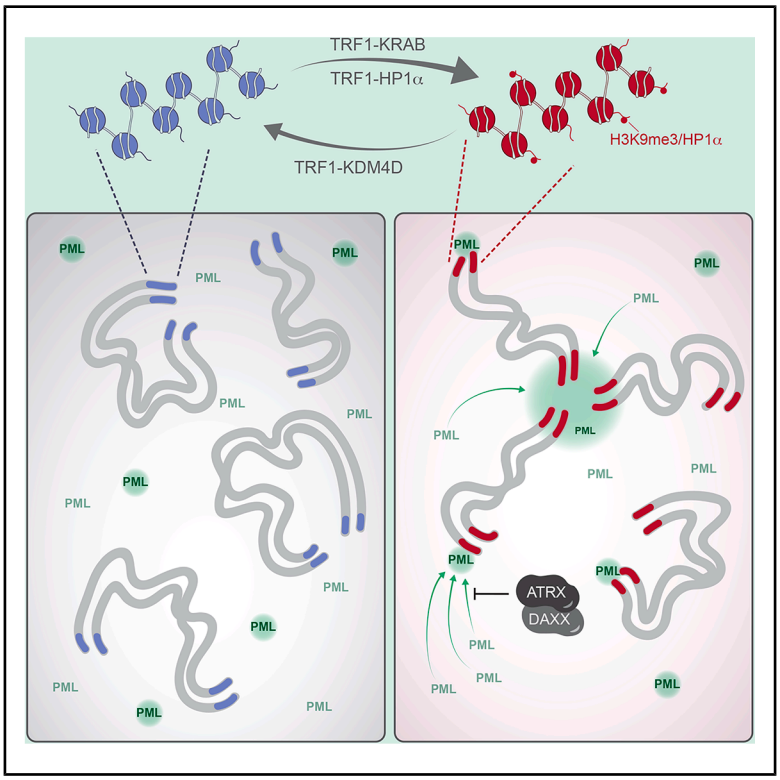


## Highlights

- Telomeric heterochromatin promotes telomere clustering and APB formation in ALT-positive cells
- HP1α tethering to TRF1 is sufficient to induce PML nuclear body formation at telomeres
- ATRX and DAXX inhibit heterochromatin-driven telomere nuclear body assembly

## Authors

Erin R. Taylor, Bruce Proctor III, Melina Vaurs, ..., Maya Raghunandan, Anabelle Decottignies, Nausica Arnoult

## Correspondence

nausica.arnoult@colorado.edu

## In brief

Telomeres in ALT-positive cancers display reduced nucleosome density yet retain heterochromatin-associated factors. This study shows that telomeric heterochromatin drives telomere clustering and PML nuclear body assembly, while ATRX and DAXX suppress this process, establishing a role for telomeric chromatin in mediating ALT-associated subnuclear compartmentalization of telomeres.

Taylor et al., 2026, Cell Reports *45*, 117004
March 24, 2026 
https://doi.org/10.1016/j.celrep.2026.117004

CellPress

Cell Reports

CellPress
OPEN ACCESS

Article

# Local heterochromatin enrichment promotes telomere clustering and PML nuclear body assembly at telomeres

Erin R. Taylor,[1,6] Bruce Proctor III,[1,6] Melina Vaurs,[2] Guanhui Wu,[3,4] Manon Mahieu,[2] Shreya Shrestha,[1] Daniel Morrison,[1] Laila Weatherly,[1] Shane Brelinsky,[1] Maya Raghunandan,[2,5] Anabelle Decottignies,[2] and Nausica Arnoult[1,7,*]

[1]Department of Molecular, Cellular and Developmental Biology, University of Colorado Boulder, Boulder, CO 80309, USA
[2]de Duve Institute, UClouvain, 1200 Brussels, Belgium
[3]Department of Biochemistry, University of Colorado Boulder, Boulder, CO 80303, USA
[4]BioFrontiers Institute, University of Colorado Boulder, Boulder, CO 80303, USA
[5]Present address: Indian Institute of Science, Bangalore 560012, India
[6]These authors contributed equally
[7]Lead contact
*Correspondence: nausica.arnoult@colorado.edu
https://doi.org/10.1016/j.celrep.2026.117004

## SUMMARY

The alternative lengthening of telomeres (ALT) pathway is a recombination-based telomere maintenance mechanism used by a subset of human cancers and is characterized by telomere clustering within telomere-associated promyelocytic leukemia (PML) nuclear bodies (APBs). Although ALT telomeres exhibit reduced nucleosome density, they are paradoxically enriched for heterochromatin-associated factors, raising questions about how chromatin state contributes to ALT. Here, we use a targeted system to locally modulate heterochromatin features at telomeres. We show that telomeric heterochromatin promotes telomere clustering and multiple hallmarks of APB-associated telomere processing in ALT-positive (ALT+) cells. Remarkably, molecular tethering of HP1α at telomeres is sufficient to nucleate PML nuclear bodies in non-ALT cells and, in specific contexts, induce biomarkers of ALT-like recombination. We further demonstrate that heterochromatin-driven PML-telomere colocalization is inhibited by α-thalassemia/mental retardation, X-linked and death domain-associated protein (ATRX/DAXX), factors frequently mutated in ALT+ tumors. Together, these findings establish telomeric heterochromatin as a driver of telomere clustering and PML nuclear body assembly, shaping ALT-associated subnuclear compartmentalization.

## INTRODUCTION

The alternative lengthening of telomeres (ALT) pathway is a telomerase-independent telomere maintenance mechanism used by a subset of human cancers to sustain replicative immortality.[1,2] ALT is a recombination-based process that extends telomeres through a conservative DNA synthesis mechanism resembling break-induced replication.[3,4] One hallmark of ALT is the presence of ALT-associated promyelocytic leukemia (PML) nuclear bodies (APBs), which are defined by the colocalization of telomeres with PML nuclear bodies (PML-NBs) and are thought to function as specialized compartments for telomere synthesis.[5,6] ALT is frequently associated with the loss of chromatin regulators, most notably the ATRX (α-thalassemia/mental retardation, X-linked) and DAXX (death domain-associated protein) complex, which deposits histone H3.3 at heterochromatic regions.[7] However, loss of ATRX or DAXX is not sufficient to induce ALT,[8] and how ATRX loss may impact chromatin regulation to contribute to the pathway remains unclear.

In higher eukaryotes, telomeres are packaged into highly compact nucleosome arrays,[9] resulting in their classification as heterochromatin domains. However, the distribution of classical epigenetic marks at telomeres does not consistently follow canonical patterns associated with compaction.[10] By contrast, ALT-positive (ALT+) telomeres exhibit a markedly less compact chromatin structure, characterized by reduced nucleosome density, a feature proposed to facilitate recombination.[11] Consistent with this, ATRX loss derepresses subtelomeric regions, increasing telomeric transcription[12] and elevating replication stress.[13] Experimental chromatin relaxation, via subtelomeric hypomethylation,[14] Suv39h1/2 deletion,[15] or histone chaperone depletion[16] also enhances ALT activity. These findings support a model in which reduced telomeric heterochromatin promotes ALT by facilitating recombination and increasing replication stress.

While it is well established that ALT telomeres have reduced histone density, the status of histone modifications remains controversial. On the one hand, studies of spontaneously immortalized primary cells found no difference in the

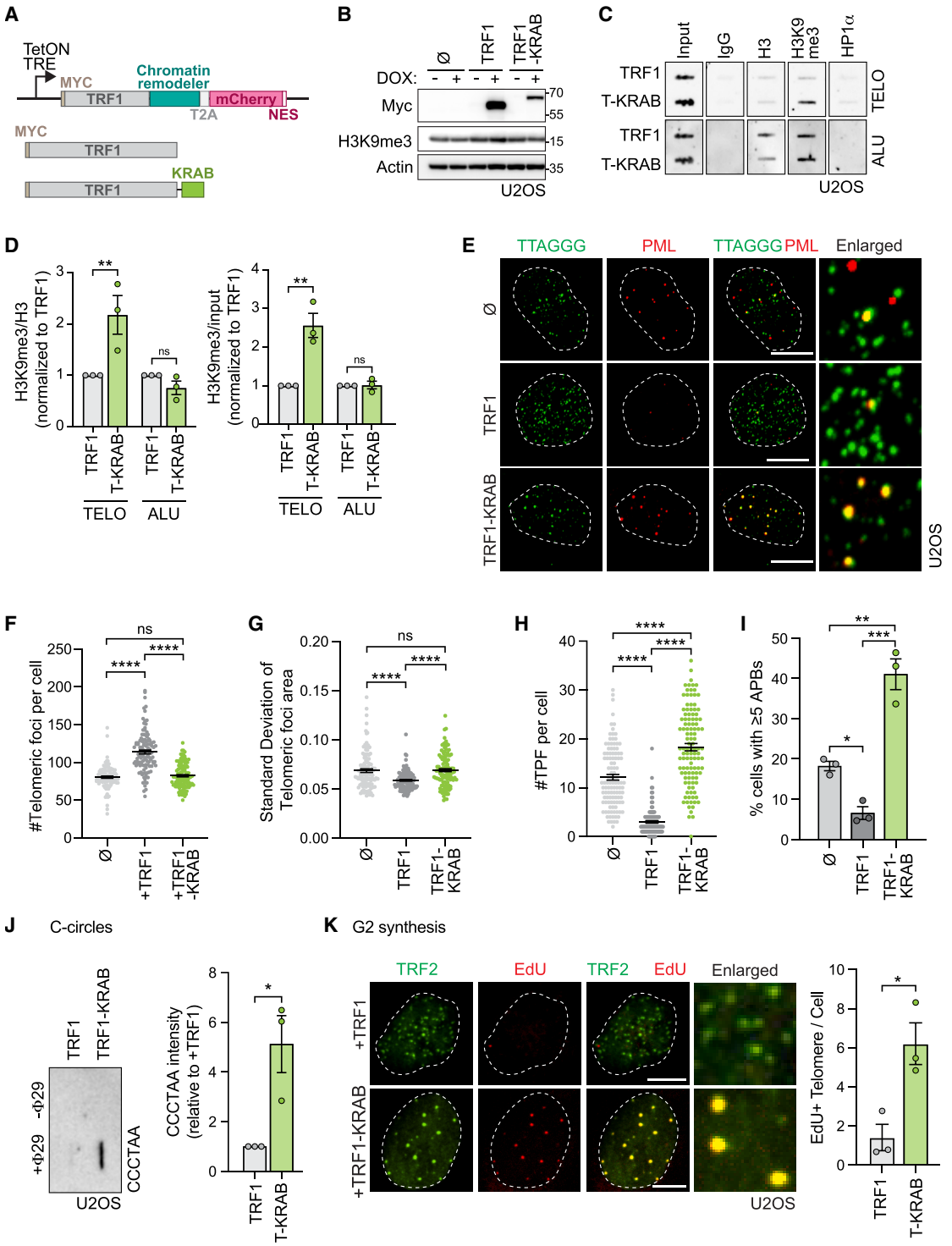


**Figure 1. Local enrichment in H3K9me3 at telomeres promotes ALT hallmarks in ALT+ cells**

(A) Schematic of the fusion-protein constructs. Top: full constructs contain a TetON doxycycline (DOX)-inducible promoter, a Myc-tagged-TRF1 fused to a chromatin modifier (here, KRAB), a T2A, and mCherry-NES (nuclear export signal).

(B) Western blot showing expression of the constructs (anti-Myc antibody) and H3K9me3 global levels in U2OS after 3 days of DOX induction.

(C) Representative chromatin immunoprecipitation of H3, H3K9me3, and HP1α at telomeres and ALU repeats in U2OS after 3 days of DOX induction (T-KRAB: TRF1-KRAB).

(D) Quantification of (C). Data represent mean ± SEM of $n = 3$ independent biological replicates.

*(legend continued on next page)*

levels of the heterochromatin-associated histone modification H3K9me3 between ALT+ and telomerase-positive derivatives, suggesting that H3K9me3 may not distinguish these states.[11] On the other hand, chromatin immunoprecipitation (ChIP)-sequencing data suggest that ALT+ tumor-derived cells may exhibit enriched H3K9me3 at telomeres.[17] Furthermore, multiple studies have shown that ALT telomeres are enriched in factors associated with constitutive heterochromatin, such as the H3K9 methyltransferase SETDB1, HP1 proteins, and KAP1 (TRIM28).[15,18–20]

Whether this enrichment in heterochromatin-associated factors at ALT telomeres promotes or restrains ALT activity remains unclear, as depletion of these chromatin regulators has produced inconsistent and at times contradictory effects on ALT activity. For example, loss of SETDB1 was shown to reduce telomeric H3K9me3 and suppress ALT activity, whereas depletion of KAP1, known to stabilize SETDB1, was observed to promote some ALT markers, while restricting others, indicating a more complex regulatory function.[15,19] Similarly, telomeric HP1α has been implicated as both a positive and negative regulator of ALT depending on the experimental context.[21,22] These conflicting outcomes are difficult to interpret, in part because genetic perturbations of chromatin regulators affect the entire genome, making it challenging to isolate telomere-specific effects. Thus, the direct role of telomeric heterochromatin in regulating ALT remains an open question.

To address this, we developed a system to locally recruit heterochromatin-promoting factors or reconstitute heterochromatin-associated features directly at telomeres without globally perturbing chromatin regulators. Using this targeted approach, we show that local heterochromatin enrichment at telomeres is sufficient to promote multiple biomarkers of APB-associated telomere processing in ALT-positive cells and that direct tethering of HP1α can induce ALT-like recombination features in non-ALT cells in a context-dependent manner. We find that HP1α tethering is sufficient to drive *de novo* PML-NB nucleation at telomeres, while ATRX/DAXX actively suppresses PML-NB formation at heterochromatin-enriched telomeres. Conversely, targeted removal of telomeric H3K9me3 disrupts telomere clustering and alters APB assembly, demonstrating that heterochromatin is required for the higher-order telomere organization characteristic of ALT. Together, these findings demonstrate that telomeric heterochromatin actively drives telomere clustering and PML-NB nucleation. However, our work also indicates that this is not sufficient to ensure recombination or productive telomere elongation, suggesting that additional determinants are required to promote recombination and productive telomere synthesis.

## RESULTS

### A fusion-protein system for local enrichment of H3K9me3 at telomeres

To investigate how local chromatin state influences ALT activity, without broadly perturbing chromatin across the genome, we developed a targeted system to recruit endogenous heterochromatin machinery directly to telomeres. Specifically, we fused the minimal Krüppel-associated box (KRAB) domain to the telomeric binding protein TRF1 (Figure 1A).[23] TRF1-fusion proteins have been previously used to site-direct various factors to telomeres,[24–27] including a TRF1-HP1α fusion which showed no perturbation of TRF2.[27] The KRAB domain is known to promote H3K9me3 accumulation by recruiting KAP1, a scaffolding protein that in turn recruits several factors, including SETDB1, an H3K9-specific methyltransferase, and HP1 proteins, which bind H3K9me3 and contribute to heterochromatin establishment.[28] Notably, KAP1, SETDB1, and HP1α have all been reported to be enriched at ALT+ telomeres.[15,18,19] We therefore reasoned that expression of TRF1-KRAB would further enhance the heterochromatic environment naturally associated with ALT+ telomeres.

To test this, we expressed Myc-tagged-TRF1 or Myc-tagged-TRF1-KRAB from a doxycycline-inducible promoter using a lentiviral vector. Additionally, we tagged the C terminus of each construct with a self-cleaving T2A peptide and a nuclear export signal (NES)-tagged mCherry to ensure comparable expression levels (Figure 1A). Constructs were transduced into ALT+ U2OS cells, expression was induced with doxycycline, and confirmed by Myc-tag Western blotting, while mCherry fluorescence was quantified by flow cytometry to assess single-cell induction heterogeneity (Figures 1B and S1A). We confirmed that the TRF1-KRAB fusion protein localized appropriately to telomeres by performing Myc-tag immunofluorescence (IF) combined with telomere fluorescence *in situ* hybridization (telo-FISH) (Figure S1B). Finally, we performed telomeric ChIP and found that expression of TRF1-KRAB resulted in the enrichment of H3K9me3 at telomeres, confirming that the KRAB domain was functional and sufficient to locally increase heterochromatin marks at these sites (Figures 1C and 1D). Notably, this enrichment was telomere-specific, as H3K9me3 was not increased at Alu repeats and no changes were observed in global H3K9me3 levels (Figures 1B–1D).

(E) Representative images of IF-FISH assessing PML colocalization with telomeres (TTAGGG) in U2OS after 3 days of DOX induction. Scale bars, 10 μm.
(F–I) Quantification of (E). (F) Number of telomere foci per cell. (G) Standard deviation of the telomere foci area within each cell. (H) Number of total (small and large) telomere-PML colocalizations (TPF). (I) percentage of cells with at least 5 APBs. (F–H) Data represent mean ± SEM of all cells analyzed over three biological replicates. *n* (number of cells analyzed) = 110 (WT), 115 (TRF1), and 113 (TRF1-KRAB). (I) Data represent mean ± SEM of *n* = 3 independent biological replicates, with at least 30 cells analyzed per replicate.
(J) Representative C-circle assay in U2OS after 3 days of DOX induction. Right: quantification. Data represent mean ± SEM of *n* = 3 independent biological replicates.
(K) G2 telomere synthesis: colocalization of TRF2 with G2-incorporated EdU in U2OS after 3 days of DOX induction. Scale bars, 10 μm. Right: quantification. Data represent mean ± SEM of 3 independent biological replicates, with at least 30 cells analyzed per replicate.
Statistical analyses: for (D and F–I), ordinary one-way ANOVA. For (J and K), Welch's *t* test. $^{*}p < 0.05$, $^{**}p < 0.01$, $^{***}p < 0.001$, and $^{****}p < 0.0001$. ns, non-significant.
See also Figure S1.

### Telomeric H3K9me3 enrichment promotes APB formation and additional ALT hallmarks in ALT+ cells

With this system, we tested whether TRF1-KRAB-mediated enrichment of H3K9me3 at telomeres alters ALT activity by measuring the levels of multiple ALT-associated biomarkers. Following doxycycline inductions for 3 days, we performed telo-FISH combined with IF against PML to assess the levels of APBs. Notably, ectopic expression of TRF1 alone reduced the baseline levels of APBs and telomere clustering, indicated by a substantial reduction in colocalization events between telo-FISH and PML-IF foci and more numerous telo-FISH foci in interphase nuclei that show less variability in size (Figures 1F–1I). This may reflect the known role of TRF1 in facilitating telomere replication,[29,30] as replication stress has been demonstrated to promote ALT activity and APBs.[31] However, the expression of TRF1-KRAB recovered endogenous foci number and size distribution, indicating that heterochromatin enrichment rescues ALT-associated clustering in a TRF1 overexpression background (Figures 1F and 1G). TRF1-KRAB expression also led to an increase in telomere-PML colocalization in U2OS, whether compared to control cells or to TRF1-expressing cells (Figures 1H and 1I). Of note, while the term APB is often used broadly to describe any colocalization between telomere FISH signal and PML foci, the original description of APB structures in ALT-positive cells emphasized enlarged, high-intensity telomeric foci, thought to reflect telomere aggregation that colocalizes with PML-NBs.[5] Here, we observed increases upon TRF1-KRAB induction of both the percentage of cells displaying $\geq$5 large colocalized foci (Figure 1I), a criteria that has previously been used to define APBs[16,32] as well as the total number of colocalized PML-telomere (Figure 1H), which includes both small and large overlapping foci (hereafter referred to as colocalized telomere-PML foci or TPF). We also found increased APB+ cells upon expression of TRF1-KRAB in SAOS2, another ALT+ osteosarcoma-derived cell line, as well as VA13, an ALT+ *in vitro* immortalized fibroblast line (Figures S1C–S1F).[33,34]

ALT+ cells are also characterized by the presence of several different species of extrachromosomal telomeric repeats (ECTRs), including partially double-stranded circles of C-rich telomeric DNA, known as C-circles.[35] We performed a C-circle assay in U2OS and VA13 cells 3 days after doxycycline induction and found that TRF1-KRAB expression also led to a significant increase in C-circles in both cell lines (Figures 1J, S1G, and S1H).

Telomere elongation in ALT cells is mediated by break-induced replication, which can be measured by 5-ethynyl-2'-deoxyuridine (EdU) incorporation at telomeres during G2 and mitosis.[2] To assess this, we synchronized doxycycline-induced U2OS cells in G2, pulsed them with EdU, and quantified EdU-telomere colocalizations in G2-phase nuclei. Consistent with the increase in APBs and C-circles, the expression of TRF1-KRAB led to a significant increase in telomeric DNA synthesis in G2 (Figure 1K). In contrast, when we synchronized cells in mitosis and measured mitotic EdU incorporation at telomeres on metaphase spreads, we observed no increase in telomeric synthesis in TRF1-KRAB-expressing cells (Figures S1I and S1J), suggesting that KRAB-mediated heterochromatin state specifically promotes G2-phase break-induced telomere synthesis rather than mitotic synthesis. It was recently demonstrated that ALT+ cells engage in both productive and non-productive telomere synthesis, with non-productive synthesis occurring during G2-phase within APBs and leading to the generation of C-circles and ECTRs, and productive telomere extension occurring at the G2-M boundary or into mitosis.[31] The phenotypes we observe upon telomeric heterochromatin enrichment appear to be consistent with promoting the former, suggesting that heterochromatin promotes the formation of APBs and the processing of telomeres within these structures.

### Direct enrichment in telomeric HP1α promotes ALT hallmarks in ALT+ cells

As a complementary approach, we also tested the impact of expressing TRF1 fused directly to HP1α, a major H3K9me3 reader that is itself a key structural component of constitutive heterochromatin through dimerization-driven chromatin bridging and recruitment of additional heterochromatin-associated partners.[36–38] Unlike TRF1-KRAB, which relies on the recruitment of histone modifiers to establish H3K9me3, direct HP1α tethering should reconstitute certain features of constitutive heterochromatin directly, bypassing the requirement for the recruitment of regulators, as well as negative regulation by demethylases and other factors.

TRF1-HP1α fusion proteins have previously been used to study the function of heterochromatin at telomeres, although their effects on ALT activity were not examined.[27] Because wild-type (WT) HP1α can bind H3K9me3 with high affinity, TRF1-HP1α can be recruited to pre-existing H3K9me3-enriched chromatin throughout the genome, rather than delivering HP1α specifically to the telomeres.[27] To avoid this, we used a mutant version of HP1α (V22M) that disrupts its interaction with H3K9me3 and thereby restricts the protein's localization to telomeric repeats (Figures 2A and S2A).[27,39]

Constructs were transduced into ALT+ U2OS cells, and expression was induced with doxycycline. The fusion protein expression was confirmed by Myc-tag Western blotting, telomere localization was validated with Myc-tag IF combined with telo-FISH, and telomere-specific chromatin remodeling was demonstrated with ChIP (Figures 2B–2D and S2B). We then tested whether direct tethering of HP1α to telomeres would phenocopy the increase in ALT features observed with TRF1-KRAB. Indeed, we found that TRF1-HP1α expression led to a significant increase in APBs, C-circles, and G2-phase telomere synthesis (Figures 2E–2H). However, TRF1-HP1α-expressing cells also showed marked differences compared with TRF1-KRAB cells. We noticed a more heterogeneous population, with some cells displaying smaller, more uniform, telo-FISH foci and very few colocalization events, reminiscent of TRF1-expressing cells, while others showed many large APBs, including some ultra-bright APBs similar to the exacerbated, "hyper-ALT" phenotype observed upon FANCM depletion in ALT+ cells (Figures 2I–2K).[40,41] We also noticed the presence of bulky telomere entanglements in a subset of cells (Figures 2J and 2L). These entanglements differ from more commonly observed telomeric, ultra-fine, anaphase bridges[42,43] in that they persist into interphase as prominent telomere-FISH bridges between daughter nuclei, consistent with robust chromatin bridging. Additionally, these entanglements were rarely observed in cells positive for APBs

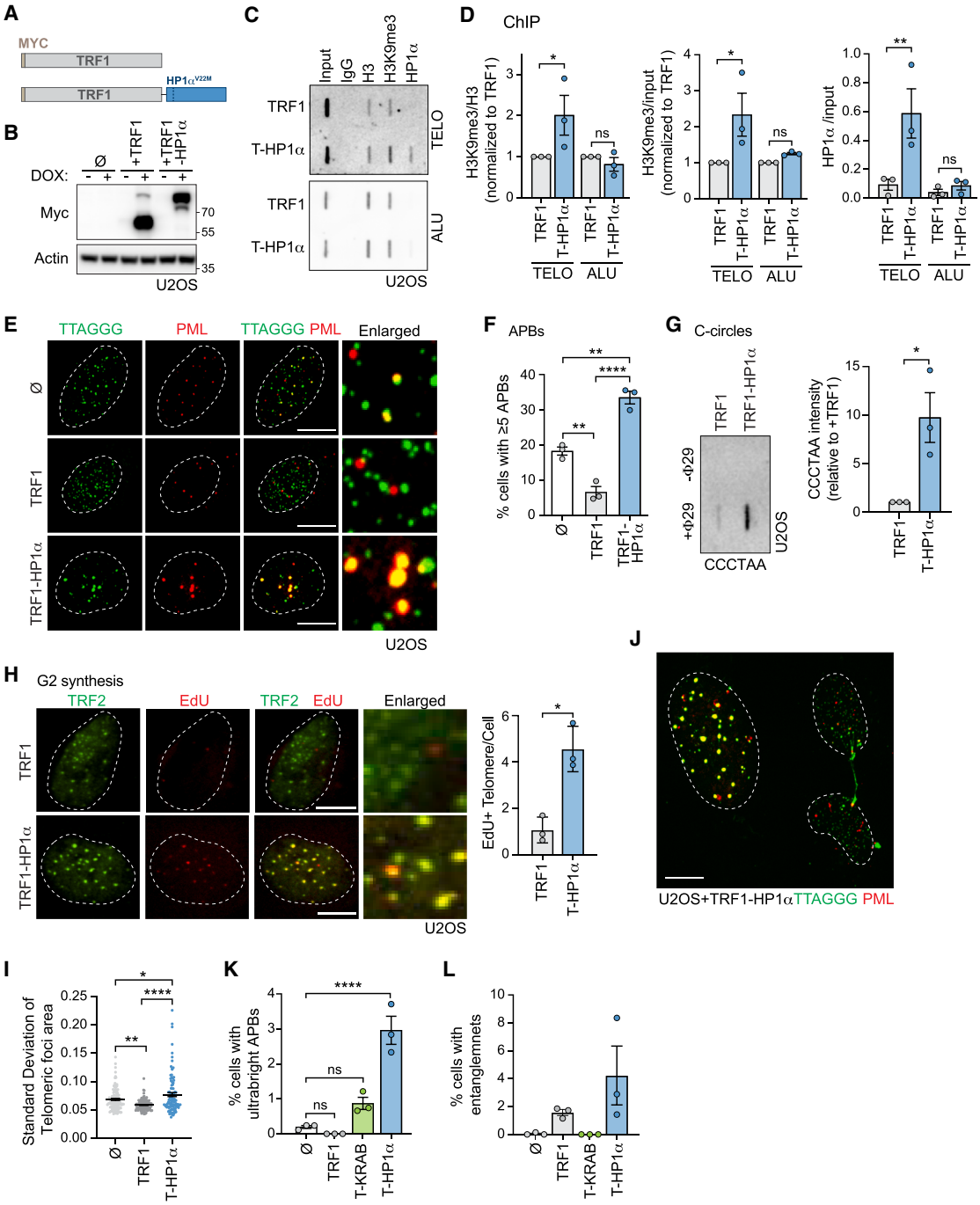


**Figure 2. Direct enrichment in telomeric HP1α promotes ALT hallmarks in ALT+ cells**

(A) Schematic of the fusion-protein constructs. Here, Myc-TRF1 is fused to HP1α V22M, a mutation that abrogates H3K9me3 binding.

(B) Western blot showing the expression of the constructs (anti-Myc antibody) in U2OS after 3 days of DOX induction.

(C) Representative chromatin immunoprecipitation of H3, H3K9me3, and HP1α at telomeres and ALU repeats in U2OS after 3 days of DOX induction (T-HP1α: TRF1-HP1α).

(D) Quantification of (C). Data represent mean ± SEM of $n = 3$ independent biological replicates.

(E) Representative images of IF-FISH assessing PML colocalization with telomeres (TTAGGG) in U2OS after 3 days of DOX induction. Scale bars, 10 μm.

(F) Quantification of cells with at least 5 APBs from (E). Data represent mean ± SEM of $n = 3$ independent biological replicates, with at least 30 cells analyzed per replicate.

(G) Representative C-circle assay in U2OS after 3 days of DOX induction. Right: quantification. Data represent mean ± SEM of $n = 3$ independent biological replicates.

*(legend continued on next page)*

and were never observed between nuclei exhibiting ultra-bright APBs, potentially indicating an inverse relationship between these phenotypes (Figure 2J).

HP1α is composed of a chromodomain (CD), which binds H3K9me3, a central hinge region, and a chromoshadow domain (CSD), which mediates dimerization and ligand binding (Figure S2A).[44] To dissect which domain is responsible for promoting ALT hallmarks, we expressed split HP1α fusion constructs in U2OS cells (Figures S2C–S2E). We found that the CSD, but not the CD + hinge region, was sufficient to promote APB formation and C-circle accumulation (Figures S2F–S2H), suggesting that dimerization, potentially with endogenous HP1α, and/or ligand binding is required to promote ALT hallmarks. Importantly, the CSD does not encompass the V22 residue, indicating that the V22M mutation itself is not a driver of the phenotype.

Ultimately, we observe that direct tethering of HP1α strongly promotes telomere clustering, APB formation, and other ALT-associated markers. However, the heterogeneity in phenotype severity and presentation across cells suggests that HP1α-driven effects may reflect properties intrinsic to its tethering rather than a uniform response to heterochromatin establishment. To better understand the overlapping yet distinct phenotypes generated by TRF1-KRAB and TRF1-HP1α in ALT+ cells, we next induced these constructs in non-ALT cells to assess which features reflect intrinsic molecular functions of the experimental systems and which depend on an ALT+ cellular context.

## Heterochromatin mediates low levels of telomere-PML colocalization foci in non-ALT cells

While APBs are considered specific to and indicative of ALT activity, PML-NBs have been shown to localize to telomeres in contexts outside of ALT. Notably, telomerase-positive cells with long telomeres were previously demonstrated to exhibit some levels of telomere-PML colocalization.[45] Since long telomeres display higher H3K9me3 levels,[46] it is possible that enriched heterochromatin at long telomeres promotes their colocalization with PML proteins. To test this hypothesis, we modulated heterochromatin in isogenic cells with long and short telomeres, and quantified TPF. We used HeLa 1.2.11, a subclone of HeLa 1.3 with long telomeres (hereafter referred to as HeLa LT),[47] and compared it to HeLa S3, a HeLa clone with short telomeres (hereafter referred to as HeLa ST). As previously reported, we found that the basal levels of TPF were significantly higher in HeLa LT than HeLa ST (Figure 3A).[45] Expression of TRF1-KRAB increased the levels of TPF, while TRF1 alone had no effect (Figures 3B and S3A–S3D). Conversely, the knockdown of HP1α reduced TPF in HeLa LT in both basal conditions and upon TRF1-KRAB expression (Figures 3C and 3D). These data indicate that heterochromatin mediates the physiological telomere-PML colocalizations observed in non-ALT cells.

## Expression of TRF1-HP1α induces multiple ALT hallmarks in non-ALT cells with long telomeres

We next tested whether TRF1-HP1α similarly increases the baseline of TPF in HeLa cells. As expected, TRF1-KRAB and TRF1-HP1α both increased telomeric levels of H3K9me3 and HP1α (Figures S3C and S3D). Consistent with the foci observed in ALT+ cells, we observed a robust induction of telomere-associated PML-NBs in HeLa LT cells expressing TRF1-HP1α (Figures 3E, 3F, and S3A–S3D). Notably, depletion of SETDB1 with small interfering RNAs (siRNAs) did not reduce these TPF, indicating that HP1α itself, rather than H3K9me3, drives the phenotype (Figures S3E and S3F). In ALT+ cells, APBs are characterized by the recruitment of the BTR (BLM-TOP3A, RMI) complex.[48] Consistent with this, BLM was readily detected at TRF1-HP1α-induced TPF in HeLa LT cells (Figure S3G). Strikingly, TRF1-HP1α, but not TRF1-KRAB, also induced high levels of C-circles (Figures 3G and S3H-I), G2-phase telomeric EdU incorporation (Figures 3H and 3I), and entanglements (Figure 3J). Finally, similar to U2OS, TRF1-tethering of HP1α CSD domain, but not of the CD + hinge, was sufficient to drive the phenotype, while expression of TRF1-HP1α I165A, a mutation that disrupts both the dimerization and ligand binding of HP1α,[49] failed to induce telomere-PML colocalizations (Figures S3J–S3L). Together, these findings indicate that TRF1-HP1α expression is sufficient to induce comparable ALT-associated phenotypes in HeLa LT cells, as was observed in U2OS.

Prior studies have shown that disruption of chromatin assembly, such as through ASF1 depletion, can trigger ALT-like features in cell lines with long telomeres but fails to do so in cell lines with shorter telomeres.[16] However, we found that expression of TRF1-HP1α led to robust induction of TPF in HeLa ST (Figures 3K and 3L), indicating that TRF1-HP1α induces telomere-PML colocalization independently of telomere length. Yet, there were notable differences between HeLa LT and HeLa ST. Although high, the number of TPF was lower in HeLa ST than in HeLa LT (Figures 3E, 3F, 3K, and 3L). We also observed very few entanglements (Figure 3M) and no induction of C-circles upon expression of TRF1-HP1α in HeLa ST (Figure S3M). Therefore, while TRF1-HP1α is sufficient to induce localization of PML-NBs at telomeres independent of telomere length, we only observed C-circles and entanglements in cells with long telomeres.

(H) G2 telomere synthesis: colocalization of TRF2 with G2-incorporated EdU in U2OS after 3 days of DOX induction. Left: representative images. Scale bars, 10 μm. Right: quantification. Data represent mean ± SEM of $n = 3$ independent biological replicates, with at least 30 cells analyzed per replicate.
(I) Quantification from (E) of the standard deviation between telomeric foci area within each cell. Data represent mean ± SEM of all cells from 3 independent biological replicates. $n$ (number of cells analyzed) = 110 (WT), 115 (TRF1), and 100 (TRF1-HP1α).
(J) Representative image from experiment in (E) of a cell with ultra-bright APBs (left) and cells with a telomeric bridge (right) in U2OS + TRF1-HP1α. Scale bar: 10 μm.
(K and L) Percentage of cells with ultra-bright APBs (K) and entanglements (L). Data represent mean ± SEM of 3 independent biological replicates, with at least 30 cells analyzed per replicate.
Statistical analyses: for (D, F, I, and K–L), ordinary one-way ANOVA. For (G and H), Welch's $t$ test. *$p < 0.05$, **$p < 0.01$, and **$p < 0.0001$. ns, non-significant. See also Figure S2.

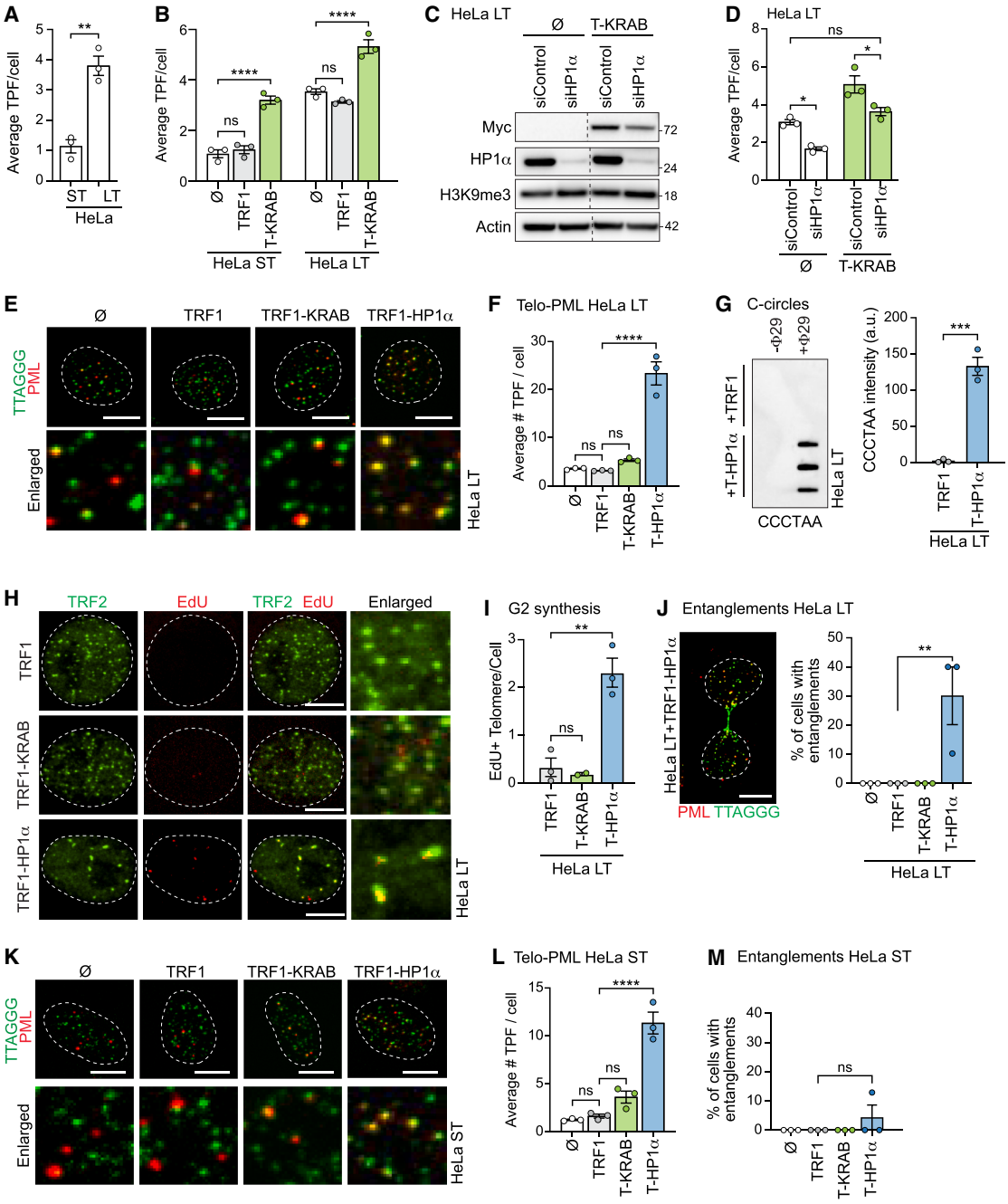


**Figure 3. Expression of TRF1-HP1α induces multiple ALT hallmarks in non-ALT cells with long telomeres**

(A) Quantification of basal levels of telomere-PML colocalization (TPF) in HeLa ST and HeLa LT. Data represent mean ± SEM of 3 independent biological replicates.

(B) Western blot showing siRNA-mediated knockdown of HP1α in HeLa LT control cells and expressing TRF1-KRAB (T-KRAB).

(C) Western blot showing Myc (TRF1-KRAB), HP1α, H3K9me3, and actin in indicated cell lines.

(D) Quantification of TPF in indicated cell lines. Data represent mean ± SEM of $n = 3$ independent biological replicates, with at least 30 cells analyzed per replicate.

(E) Representative images of IF-FISH assessing PML (IF) colocalization with telomeres (TTAGGG) in HeLa LT with indicated constructs after 3 days of DOX induction. Scale bars, 10 μm.

(F) Quantification of TPF from (E). Data represent mean ± SEM of $n = 3$ independent biological replicates, with at least 30 cells analyzed per replicate.

(G) C-circle assay in HeLa LT after 3 days of DOX induction. Data represent mean ± SEM of $n = 3$ independent biological replicates.

(H) G2 telomere synthesis: colocalization of TRF2 with G2-incorporated EdU in HeLa LT after 3 days of DOX induction. Scale bars, 10 μm.

*(legend continued on next page)*

### TRF1-HP1α-induced telomere entanglements do not depend on PML-NB recruitment

Chromatin bridging arises as a consequence of unresolved topological DNA-interlinks between sister chromatids, late replication intermediates, as well as unresolved recombination intermediates.[43] Because replication stress can produce late replication intermediates, and has been shown to promote APB formation and ALT activity in certain contexts,[31] we wanted to assess whether the telomere entanglements observed in TRF1-HP1α-expressing HeLa LT cells directly correlate with the induction of ALT-associated phenotypes. We therefore tracked the temporal dynamics of telomere entanglements and APB formation following doxycycline induction (Figures 4A and 4B). We found that the entanglements peaked at 24 h and declined thereafter, accompanied by a transient growth arrest that resolved by 36 h (Figure 4C). In contrast, telomere-PML colocalization (including BLM recruitment) remained low at 24 h and rose as entanglements diminished (Figures 4A and 4B, middle and right). At 72 h, only 5% of cells still exhibit entanglements, while 25% harbor TPF (Figure 4B, left and middle). Thus, TPF forms after entanglements have resolved, indicating that TPF is not the cause of entanglements. Supporting this conclusion, we also found that treatment with a SUMO inhibitor, which prevents PML-NB formation,[50] did not prevent entanglements (Figures 4D and 4E). Similarly, TRF1-HP1α-expressing HeLa ST cells exhibit TPF but almost no entanglements.

An alternative possibility is that APBs/TPF facilitate the resolution of aberrant telomere entanglements. Supporting this model, disruption of APB structure by ICP0* in U2OS cells was previously shown to produce telomere bridges, consistent with failure to resolve recombination intermediates.[51] Similarly, U2OS-TRF1-HP1α cells harboring entanglements lacked large APBs (Figure 2J) and ectopic TRF1 expression alone produced low levels of thin entanglements in U2OS cells (Figure 2K), potentially reflecting APB loss in this background. Notably, excessive TRF1 relative to available binding sites in mouse embryonic stem cells (mESCs) was previously reported to promote *trans* dimerization between telomeres on different chromosomes, generating multi-telomere entanglements.[52] Our data suggest that TRF1-HP1α tethering may induce analogous higher-order telomere bridging and subsequent recombination through HP1α-mediated dimerization and clustering. While the presence of entanglements correlates with biomarkers of ALT-associated recombination, strong PML-NB recruitment occurs even when recombination features are absent, indicating that HP1α tethering promotes both telomere clustering/recombination and PML recruitment but that these processes are not dependent on one another.

### TRF1-HP1α induces a persistent ALT-like state in primary cells, but not productive telomere extension

We next sought to determine whether TRF1-HP1α is sufficient to stably induce ALT hallmarks in a system that better models the physiological context in which telomere maintenance pathways are naturally activated; namely, telomerase-negative, checkpoint-deficient cells with short telomeres. To this end, we performed long-term doxycycline induction (30 days) of TRF1 or TRF1-HP1α in late-passage IMR90 E6E7 cells (Figures S4A and S4B). Remarkably, even after 30 days, TRF1-HP1α-expressing cells displayed clear telomere-PML colocalization without telomeric entanglements (Figures S4B–S4D), consistent with our findings in HeLa ST cells. Notably, at this late population doubling (∼PD95), control cells exhibited very dim telomere FISH signals, indicative of very short telomeres. In contrast, TRF1-HP1α expressing cells showed bright telomere FISH foci, suggestive of either telomere clustering, ECTRs, or elongation of a subset of telomeres (Figure S4B, left). To distinguish between these possibilities, we performed a telomere restriction fragment (TRF) assay. Although only a subset of cells (∼10%–20%) continued to express the construct after long-term induction, we reasoned that major elongation events should be detectable by TRF. However, we found no measurable difference in telomere length between the three conditions, indicating that TRF1-HP1α induces telomere clustering in PML bodies, without productive telomere elongation (Figures S4E and S4F). Similarly, we saw no measurable difference in telomere length by TRF analysis in HeLa LT cells expressing TRF1-HP1α after 3 days of induction, nor at 2 weeks, compared to uninduced control cells (Figure S4G).

Together, these findings show that tethering of HP1α to telomeres is sufficient to induce local PML-NB assembly, telomere clustering, and in certain contexts, phenotypes consistent with ALT-like recombination but does not support productive ALT-mediated telomere extension.

### HP1α interaction with SP100 does not drive the TRF1-HP1α-mediated APB increase in ALT+ cells

One possible mechanism by which TRF1-HP1α induces TPF could be through a direct interaction with a PML-NB component. A compelling candidate for this is SP100, a core component of PML-NBs, known to be a direct interactor of HP1α.[53] However, the role of SP100 in ALT is complex. A prior study in ALT+ cells demonstrated that SP100 overexpression suppresses APB formation and telomeric recombination by sequestering the MRE11/RAD50/NBS1 (MRN) complex away from PML bodies, suggesting that SP100 acts as a negative regulator of ALT.[54] To delineate the role of SP100 in the TRF1-HP1α-mediated

(I) Quantification of (H). Data represent mean ± SEM of $n = 3$ independent biological replicates, with at least 30 cells analyzed per replicate.
(J) Representative image and quantification of entanglements in HeLa LT with indicated constructs. Data represent mean ± SEM of $n = 3$ independent biological replicates, with at least 30 cells analyzed per replicate. Scale bar: 10 μm.
(K) Representative images of IF-FISH assessing PML (IF) colocalization with telomeres (TTAGGG) in HeLa ST with indicated constructs after 3 days of DOX induction. Scale bars, 10 μm.
(L and M) Quantification of TPF (L) and entanglements (M) from (K). Data represent mean ± SEM of $n = 3$ independent biological replicates, with at least 30 cells analyzed per replicate.
Statistical analyses: for (B, D, F, I, and L), ordinary one-way ANOVA. For (G, J, and M), Welch's *t* test. $^{*}p < 0.05$, $^{**}p < 0.01$, $^{***}p < 0.001$, and $^{****}p < 0.0001$. ns, non-significant. See also Figure S3.

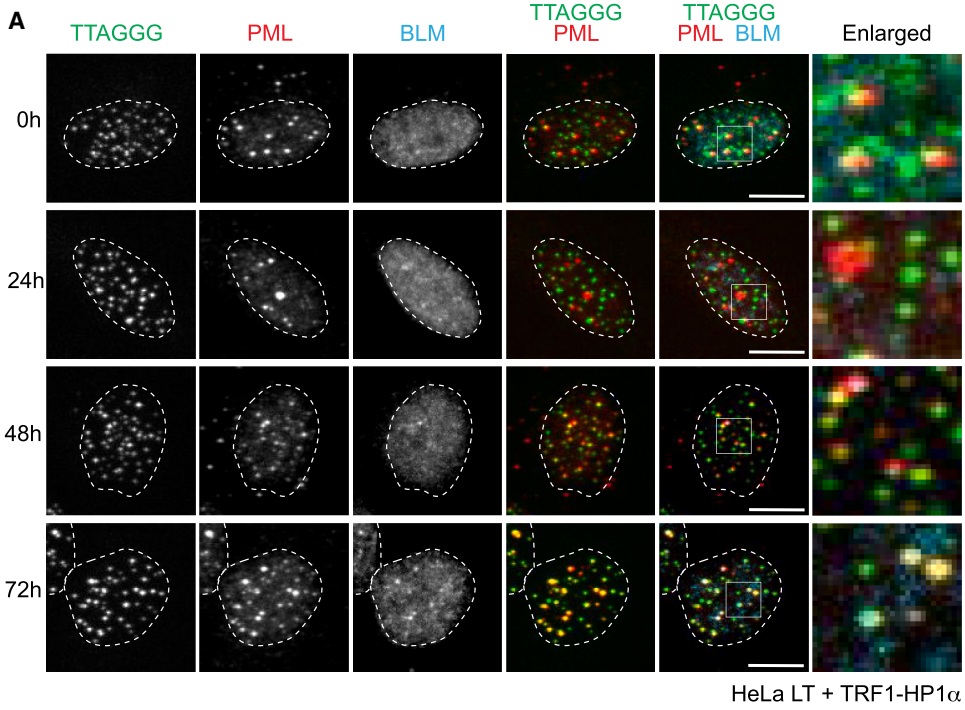


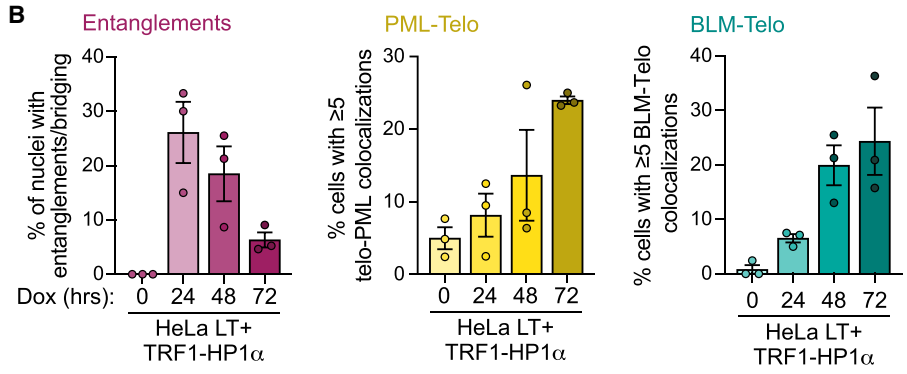


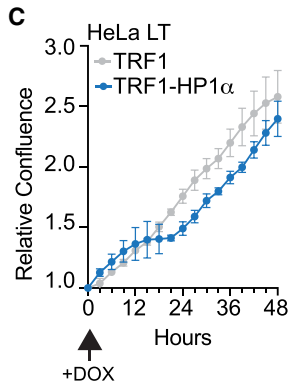


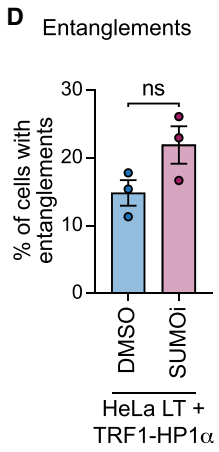


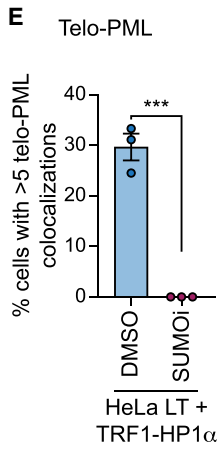


*(legend on next page)*

PML-telomere colocalization, we depleted SP100 with siRNAs in HeLa ST and U2OS prior to inducing our constructs (Figures S5A–S5C).

Knockdown of SP100 suppressed the TRF1-HP1α-mediated telomere-PML colocalizations in HeLa ST (Figure S5D and S5E). However, it also reduced the number of PML-NBs as well as PML protein levels, making these results difficult to interpret (Figures S5E–S5F). In contrast, knockdown of SP100 did not reduce the number of PML-NBs observed and resulted in increased PML protein levels in U2OS cells (Figures S5F–S5H). In this context, the TRF1-HP1α-mediated increase in APBs was further amplified, rather than suppressed, by SP100 knockdown (Figures S5G and S5H). Therefore, TRF1-HP1α is unlikely to promote TPF or APB formation through a direct SP100 interaction.

## HP1α promotes PML-NB nucleation at telomeres, which is limited by PML protein levels

PML can exist in various biochemical states (soluble, chromatin-bound, or phase-separated) depending on cell cycle stage, SUMOylation, and stress signaling.[55–57] PML-NB number does not scale linearly with PML protein levels, and can instead be modulated through redistribution or post-translational modification of pre-existing PML pools.[56,57] Furthermore, PML expression can increase in response to stress. For instance, PML and SP100 are among the top transcriptional targets of type I interferon (IFN) signaling,[58] likely due to the prominent function of PML-NBs in the viral response.[59] Thus, expression of TRF1-HP1α could either drive the nucleation of existing soluble PML proteins or lead to an increase in PML protein levels. To distinguish between these two hypotheses, we looked at PML protein levels following TRF1-HP1α expression. We found that PML levels remained unchanged upon expression of any constructs across all cell lines (Figure 5A). However, upon expression of TRF1-HP1α, we observe an increase in the total number of PML foci concurrent with a decrease in the average size of observed foci (Figures 5B and 5C), indicating that TRF1-HP1α is sufficient to drive the nucleation of existing PML to form NBs directly at telomeres, rather than the localization of telomeres to existing PML-NBs.

Although TRF1-HP1α expression induces TPF in both HeLa ST and HeLa LT, these levels remained lower in HeLa ST (∼12 in HeLa ST vs. ∼25 in HeLa LT, Figures 3F and 3L). While this difference could reflect a functional divergence dependent on telomere length, we also observed that HeLa ST cells exhibit markedly lower levels of PML protein compared to HeLa LT or U2OS (Figures 5A and S5F), which could additionally or alternatively limit TPF formation. To distinguish between these possibilities, we tested whether increasing PML levels in HeLa ST would be sufficient to increase HP1α-mediated telomere-PML colocalizations. In order to increase PML abundance in HeLa ST, we transfected cells with poly(I:C), a method to induce IFN response and activate PML transcription.[60] As expected, poly(I:C) treatment led to a marked increase in PML protein levels with all constructs (Figure 5D). Notably, poly(I:C) increased the number of telomere-PML colocalizations in HeLa ST-TRF1-HP1α, to the levels observed in HeLa LT-TRF1-HP1α (Figures 5E and 5F). To control that the observed increase in PML-telomere colocalization is a direct effect of increased PML levels rather than a response to innate immune activation, we overexpressed PML-IV—a form of PML important for APB formation[61]—in HeLa ST cells expressing TRF1-HP1α (Figures 5G and 5H). We found that the number of TPF in HeLa ST overexpressing PML increased to the levels observed in HeLa-LT-TRF1-HP1α (Figures 5H and 5I). Conversely, we targeted PML with CRISPR-Cas9 in HeLa LT and isolated clones with partial depletion of PML protein levels (Figure 5J). In this context, we observed a decrease in TPF, proportionally to the observed decrease in PML bodies (Figures 5K and 5L). These results suggest that the capacity of the two cell lines to form TPF depends on PML availability rather than telomere length. Together, these results indicate that TRF1-HP1α promotes the localization of available PML proteins to telomeres and *de novo* nucleation of NBs, a process that is limited by the level of available PML.

Strikingly, even when PML levels were elevated by poly(I:C) treatment, TRF1-KRAB remained unable to induce telomere-PML colocalizations in non-ALT cells (Figures 5D–5F). We next sought to understand why TRF1-KRAB fails to induce high levels of TPF in non-ALT cells when both constructs promote ALT hallmarks in ALT+ cells.

## ATRX prevents H3K9me3-enriched telomeres from forming APBs

The distinct phenotypes seen upon TRF1-KRAB expression compared to TRF1-HP1α in non-ALT cells cannot be explained by differential heterochromatin enrichment, as expression of both constructs in HeLa LT cells led to similar levels of both H3K9me3 and HP1α at telomeres (Figures S3C and S3D). Instead, these data suggest that in non-ALT cells, recruitment of endogenous HP1α (via TRF1-KRAB) differs functionally from its direct tethering to TRF1. Moreover, this observation indicates the presence of a mechanism in non-ALT cells that actively inhibits H3K9me3/HP1α-enriched telomeres from forming TPF.

**Figure 4. TRF1-HP1α-induced telomere entanglements do not depend on PML-NB recruitment**

(A) Representative images of IF-FISH assessing colocalization of PML and BLM with telomeres (TTAGGG) in HeLa LT + TRF1-HP1α 0, 24, 48, and 72 h after DOX induction. Scale bars, 10 μm.

(B) Quantification of (A). Left: entanglements (not shown in [A] but shown in Figure 3J), middle: telomere-PML colocalizations, and right: BLM-telomere colocalizations. Data represent mean ± SEM of $n = 3$ independent biological replicates, with at least 30 cells analyzed per replicate.

(C) Cell growth assay assessed by live microscopy in HeLa LT after induction of the indicated constructs. Data represent mean ± SD of $n = 2$ independent biological replicates.

(D and E) Quantification of entanglements and telomere-PML colocalizations in HeLa LT + TRF1-HP1α after 2 days of DOX induction and 16 h of SUMO inhibitor (SUMOi) treatment. Data represent mean ± SEM of $n = 3$ independent biological replicates, with at least 30 cells analyzed per replicate.

Statistical analyses: for (D and E), Welch's *t* test. ***$p < 0.001$. ns, non-significant. See also Figure S4.

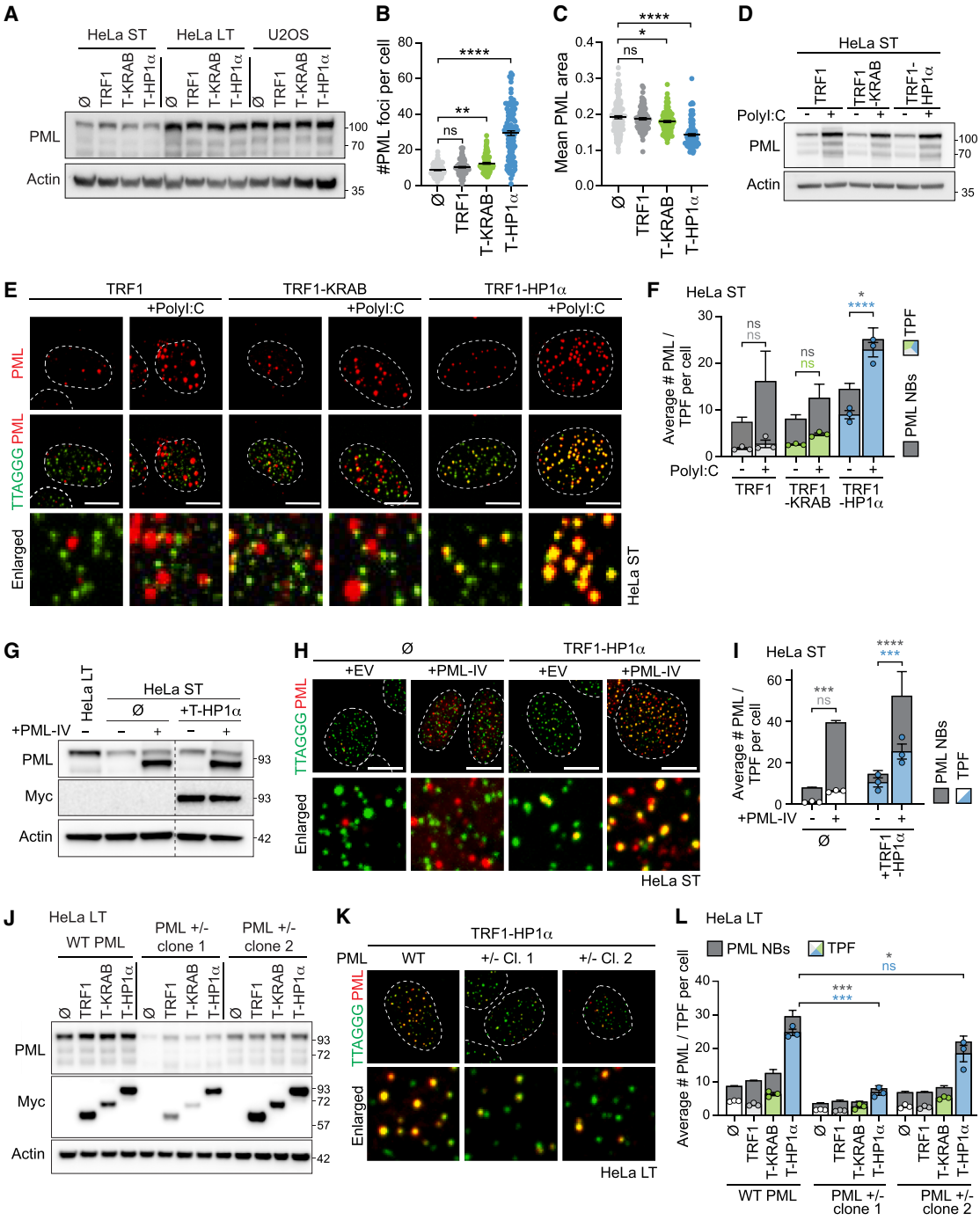


**Figure 5. HP1α promotes PML-NB nucleation at telomeres, which is limited by PML protein levels**

(A) Western blot showing PML levels in HeLa ST, HeLa LT, and U2OS upon expression of the indicated constructs. T-KRAB: TRF1-KRAB and T-HP1α: TRF1-HP1α.

(B and C) Quantification of PML foci number (B) and mean area (C) per cell in HeLa LT expressing the indicated constructs, from IF-FISH experiment in (Figure 3E). Data represent mean ± SEM of all cells from 3 independent biological replicates. *n* (number of cells analyzed) = 113 (WT), 103 (TRF1), 106 (TRF1-KRAB), and 114 (TRF1-HP1α).

(D) Western blot showing total PML protein levels in HeLa ST with the indicated constructs induced for 3 days and, when indicated, transfected with poly(I:C).

(E) Representative images of IF-FISH assessing PML colocalization with telomeres (TTAGGG) in HeLa ST expressing the indicated constructs and, when indicated, transfected with poly(I:C). Scale bars, 10 μm.

*(legend continued on next page)*

As the most recurrent genetic alteration in ALT+ tumors is the inactivation of the ATRX/DAXX chromatin remodeling complex,[7] we considered whether ATRX might prevent KRAB-mediated H3K9me3/HP1α-enriched non-ALT telomeres from nucleating PML-NBs. To test this hypothesis, we knocked down ATRX after inducing TRF1, TRF1-KRAB, and TRF1-HP1α in HeLa LT (Figures 6A–6C and S6A). Depletion of ATRX had minor effects on its own or with TRF1 expression. In contrast, ATRX suppression induced robust TPF in cells expressing TRF1-KRAB, while the increase was modest in cells expressing TRF1-HP1α (Figure 6C). We obtained similar results upon knockdown of ATRX in IMR90E6E7 cells (Figures 6D and S6A–S6C) or upon CRISPR-Cas9-mediated knockout (KO) of ATRX in HeLa LT (Figures 6E, S6D, and S6E). Finally, we also knocked down ATRX partner, DAXX, and found, again, that si-DAXX increased TPF in HeLa LT expressing TRF1-KRAB (Figures 6F–6H).

Therefore, upon ATRX suppression in non-ALT cells, TRF1-KRAB can induce high levels of TPF, indicating that ATRX actively suppresses the ability of H3K9me3/HP1α-enriched telomeres to recruit and nucleate PML-NBs, uncovering a role for ATRX/DAXX in preventing heterochromatin-driven ALT-associated subnuclear compartmentalization. However, elevated TPF levels in the absence of ATRX do not result in the presence of entanglements, nor C-circle production in TRF1-KRAB-expressing cells (Figures 6I, S6F, and S6G). Similarly, ATRX KO in HeLa ST cells expressing TRF1-HP1α increased TPF but neither induced entanglements nor C-circles (Figure S7), demonstrating that a high frequency localization of telomeres to PML-NBs is not sufficient to induce phenotypes consistent with ALT-associated recombination.

### Targeted reduction of telomeric H3K9me3 attenuates PML recruitment and telomere clustering

Having demonstrated that targeted heterochromatin enrichment is sufficient to promote telomere clustering and PML-NB seeding at telomeres, we next asked whether reducing telomeric heterochromatin through a complementary targeted approach could conversely suppress TPF formation. To remove H3K9me3 at telomeres, we fused TRF1 to the lysine demethylase KDM4D. The members of the KDM4 family (A–E) catalyze di- and tri-demethylation of H3K9 and H1.4K26; however, KDM4A–C also demethylate H3K36 and H3K56, respectively.[62,63] We therefore selected KDM4D for its specificity toward H3K9, as H1.4K26me3 has not been reported at telomeres. Although TRF1-KDM4D was expressed at notably lower levels than TRF1, it efficiently localized to telomeres and reduced telomeric H3K9me3 (Figures 7A–7E).

In HeLa LT cells, which display elevated basal TPF levels, expression of TRF1-KDM4D led to a marked reduction in TPF (Figure 7F). In contrast, TPF levels in HeLa ST cells were largely unchanged. We also examined ATRX-deficient HeLa cells, which exhibit higher baseline TPF frequencies. In this context, TRF1-KDM4D significantly reduced TPF levels irrespective of telomere length, although TPF frequencies remained higher than those observed in ATRX-proficient cells expressing TRF1-KDM4D (Figures 7D–7F). These findings suggest that ATRX loss and heterochromatin enrichment may promote PML recruitment through partially distinct mechanisms, and that while heterochromatin contributes to elevated TPF formation, it does not fully account for the increased TPF frequency observed upon ATRX loss.

Finally, we assessed the requirement for telomeric heterochromatin in APB architecture in ALT+ U2OS cells. Although TRF1-KDM4D expression did not abolish telomere-PML colocalization, it significantly altered the morphology of these colocalizations; we observed an increased number of telomeric foci, as well as more numerous, but smaller, PML foci (Figures 7G–7L). These changes indicate robust telomere declustering upon loss of H3K9me3, to an extent exceeding that observed with TRF1 expression alone, and disruption of APBs. However, telomere-PML colocalization remained elevated relative to TRF1-only controls, suggesting that while heterochromatin facilitates APB maturation and telomere clustering, it is likely not the sole determinant of APB/TPF formation in ALT+ cells.

## DISCUSSION

Here, we leverage TRF1 fusion proteins to modulate heterochromatin features specifically at telomeres and define how telomeric chromatin state influences hallmarks of ALT-associated telomere localization and processing. Enriching telomeric heterochromatin in ALT+ cell lines, through expression of either TRF1-KRAB or TRF1-HP1α, increased multiple hallmarks consistent with APB-associated telomere processing, including telomere clustering, telomere-PML colocalization, C-circle accumulation, and telomeric DNA synthesis in G2 (Figures 1 and 2). These findings indicate that telomeric heterochromatin

(F) Quantification from (C) of the number of PML NBs foci (dark gray bars) and telomere-PML colocalized foci (TPF) (light gray, green, or blue). Data show the average ± SEM of $n = 3$ biological replicates, with at least 30 cells analyzed per replicate.
(G) Western blot showing PML levels and TRF1-HP1α (Myc) expression in HeLa ST and HeLa ST + TRF1-HP1α expressing empty vector (–) or PML-IV. Control HeLa LT is shown as a reference.
(H) Representative images of IF-FISH assessing PML colocalization with telomeres (TTAGGG) in HeLa ST expressing the indicated constructs. Scale bars, 10 μm.
(I) Quantification from (F) of the number of PML NBs foci (dark gray bars) and TPF (white or blue bars). Data show average ± SEM of $n = 3$ biological replicates, with at least 20 cells analyzed per replicate.
(J) Western blot showing PML levels and TRF1-fusion constructs (Myc) expression in parental HeLa LT or in 2 clonal lines of HeLa LT with CRISPR-Cas9-mediated partial knockout of PML and expressing the indicated constructs.
(K) Representative images of IF-FISH assessing PML colocalization with telomeres (TTAGGG) in the indicated HeLa LT cell lines. Scale bars, 10 μm.
(L) Quantification from (H and I) of the number of PML NBs foci (dark gray bars) and TPF (white, light gray, green, or blue bars). Data show average ± SEM of $n = 3$ biological replicates, with at least 30 cells analyzed per replicate.
Statistical analyses for (B, C, F, I, and L), ordinary one-way ANOVA. Statistical comparisons on top refer to PML NBs, and those on the bottom refer to TPF. $^{*}p < 0.05$, $^{**}p < 0.01$, $^{***}p < 0.001$, and $^{****}p < 0.0001$. ns, non-significant. See also Figure S5.

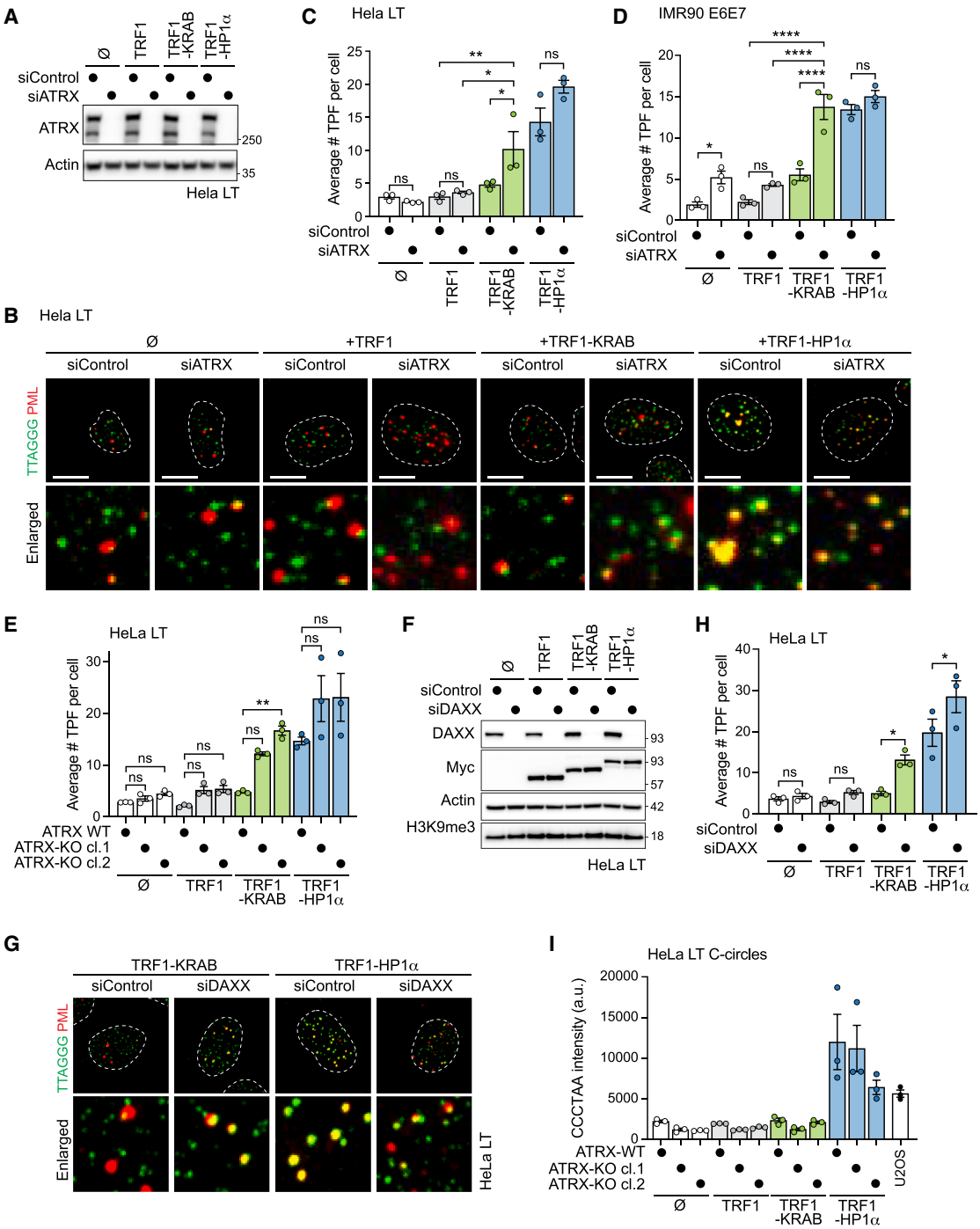


**Figure 6. ATRX/DAXX prevent H3K9me3-enriched telomeres from forming APBs**

(A) Western blot showing siRNA-mediated knockdown of ATRX in HeLa LT expressing the indicated constructs.

(B) Representative images of IF-FISH assessing PML colocalization with telomeres (TTAGGG) in HeLa LT cells in indicated conditions. Scale bars, 10 μm.

(C and D) Quantification from (B) and (Figure S6C) of telomere-PML colocalized foci (TPF) in HeLa LT (C) and IMR90 E6E7 (D) expressing the indicated constructs and transfected with control or ATRX siRNA, following the timeline described in Figure S6A. Data represent mean ± SEM of *n* = 3 biological replicates, with at least 30 cells analyzed per replicate.

(E) Quantification from (Figures S6D and E) of the number of TPF in parental and ATRX-KO clones expressing the indicated constructs. Data show average ± SEM of *n* = 3 biological replicates, with at least 30 cells analyzed per replicate.

(F) Western blot showing DAXX, Myc (TRF1-fusion constructs), and H3K9me3 in HeLa LT expressing the indicated constructs and transfected with control or DAXX siRNAs.

*(legend continued on next page)*

does not prevent ALT but rather actively promotes the clustering and subnuclear compartmentalization of telomeres within APBs, both processes are thought to support ALT-mediated telomere maintenance. Furthermore, targeted removal of telomeric H3K9me3 revealed that heterochromatin is required for both telomere clustering and normal APB architecture in ALT+ cells. Loss of telomeric H3K9me3 reduced telomere-PML colocalization frequency, disrupted APB morphology, and led to telomere declustering, although residual telomere-PML association persisted (Figure 7). Together, these findings suggest that heterochromatin facilitates robust APB assembly and higher-order telomere organization.

Several studies support this model, in which H3K9me3-linked factors contribute positively to ALT phenotypes. Notably, loss of SETDB1, either directly or through disruption of the CHAMP1 complex, reduces telomeric H3K9me3 levels and suppresses ALT activity.[15] Similarly, disruption of the CHAMP1 complex, which recruits SETDB1 to telomeres, abolishes the increase in ALT hallmarks observed following induction of double-strand breaks within ALT telomeres.[48] Our data complement these findings by demonstrating that ALT phenotypes are promoted by heterochromatin enrichment specifically at telomeres rather than by global chromatin alterations and build upon these findings by providing evidence that heterochromatin promotes ALT through telomere clustering and APB formation.

Additionally, we demonstrate that heterochromatin-mediated localization of PML-NBs to telomeres occurs outside the context of ALT. Baseline TPF in non-ALT cells with long telomeres was reduced upon depletion of HP1α or targeted removal of telomeric H3K9me3 (Figures 3D and 7F), indicating that telomeric heterochromatin underlies these endogenous telomere-PML associations. Importantly, we identify ATRX/DAXX as a key factor restraining heterochromatin-driven PML-NB assembly at telomeres. In non-ALT cells, TRF1-KRAB efficiently enriches telomeric H3K9me3 and recruits endogenous HP1α yet fails to induce high levels of telomere–PML colocalization unless ATRX/DAXX is suppressed (Figures 3 and 6). These findings indicate that one function of ATRX/DAXX in restricting ALT is to inhibit H3K9me3/HP1α-enriched telomeres from nucleating or stabilizing TPF. Given that ATRX/DAXX loss is among the most recurrent genetic alterations in ALT-associated tumors[7]; these results support a model in which loss of ATRX removes a regulatory constraint on heterochromatin-enriched telomeres, permitting PML-based compartmentalization. Consistent with this model, ATRX-mutant pediatric glioblastomas frequently harbor inactivating mutations in the H3K9/K36 demethylase KDM4B, leading to elevated telomeric H3K9me3, increased HP1α accumulation, and APB formation.[64]

While it remains unclear whether ATRX/DAXX inhibits heterochromatin-driven TPF formation directly or indirectly, the observation that direct tethering of HP1α is sufficient to bypass this inhibition and induce robust TPF across all cell lines tested is mechanistically informative. Notably, this increase in TPF was accompanied by an increase in PML-NB number without changes in total PML protein levels, demonstrating that HP1α tethering is sufficient to nucleate PML bodies *de novo* at telomeres rather than promoting relocalization to pre-existing PML-NBs (Figure 5). TRF1-HP1α expression also induced recombination-associated features, including telomere entanglements and C-circle accumulation; however, these phenotypes were observed only in specific cellular contexts outside of ALT, most prominently in HeLa LT cells.

Multiple lines of evidence support the interpretation that the telomere entanglements observed reflect clustering-mediated telomeric recombination rather than a downstream consequence of PML-NB formation. Disruption of PML-NB assembly did not suppress entanglement formation, and entanglements frequently arose prior to or in the absence of large PML-NBs. Together, these observations support a model in which heterochromatin-driven telomere clustering promotes physical proximity between telomeres, creating opportunities for recombination through higher-order interactions. In contrast, PML-NB assembly represents a distinct but parallel outcome of HP1α enrichment that is neither required for nor sufficient to initiate recombination.

Finally, our study highlights that heterochromatin-driven telomere clustering and APB-like assembly do not necessarily result in productive telomere elongation. Long-term HP1α tethering in late-passage IMR90 E6E7 cells produced persistent telomere-PML colocalization and ultrabright telomere FISH signals without measurable telomere lengthening (Figure S4). Similarly, in ALT-positive U2OS cells, telomeric heterochromatin enrichment enhanced G2-associated telomeric DNA synthesis but did not increase mitotic telomere synthesis (Figure S1). These observations are consistent with models in which ALT cells engage in both productive and non-productive telomeric synthesis, with G2-associated synthesis generating extrachromosomal telomeric repeats rather than stable extension of chromosome ends, which becomes favored as cells enter mitosis.[65] Together, these data indicate that telomeric heterochromatin primarily promotes upstream organizational and processing steps associated with APB activity rather than directly driving recombination or telomere extension.

Interestingly, while chromatin dysregulation has previously been shown to induce ALT phenotypes in non-ALT cells, this was primarily observed with perturbations that promote reduced chromatin compaction and nucleosome density, such as suppression of the histone chaperone ASF1 or inhibition of its regulators TLK1/2.[16,66] In these settings, indications of recombination and telomere extension have been observed, raising

(G) Representative images of IF-FISH assessing PML colocalization with telomeres (TTAGGG) in HeLa LT from (F) following the timeline described in Figure S6A. Scale bars, 10 μm.

(H) Quantification from (F and G) of the number of TPF in the indicated HeLa LT lines. Data show average ± SEM of $n = 3$ biological replicates, with at least 30 cells analyzed per replicate.

(I) C-circle quantification from (Figure S6F) in HeLa LT parental and ATRX-KO clones expressing the indicated constructs. Data show average ± SEM of $n = 3$ biological replicates.

Statistical analyses for (C, D, E, and H), ordinary one-way ANOVA. *$p < 0.05$, **$p < 0.01$, and ****$p < 0.0001$. ns, non-significant. See also Figures S6 and S7.

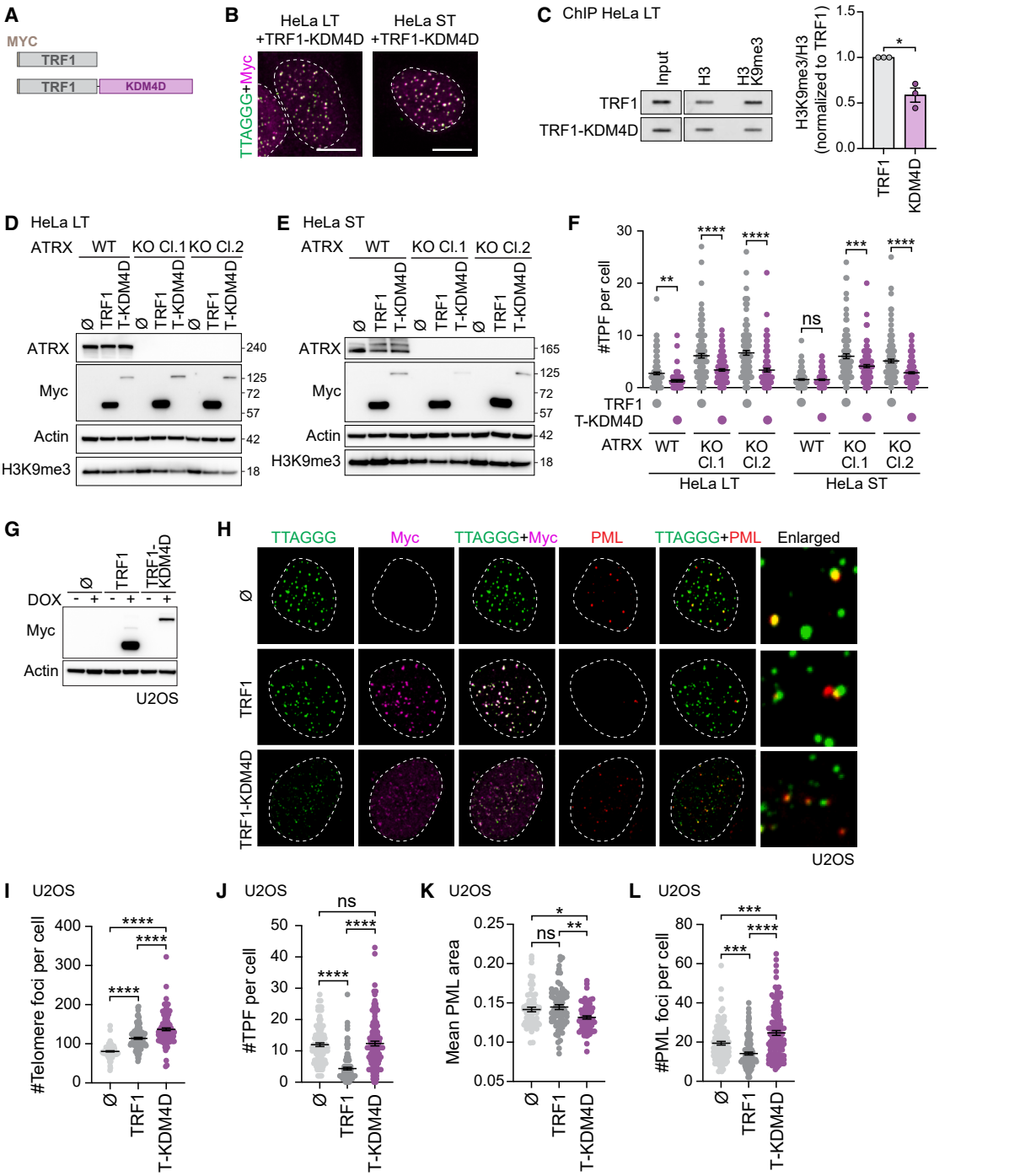


**Figure 7. Targeted reduction of telomeric H3K9me3 attenuates PML recruitment and telomere clustering**

(A) Schematic of the fusion-protein constructs. Here, Myc-TRF1 is fused to the histone demethylase KDM4D.

(B) Representative images of IF-FISH showing colocalization of the fusion-protein (anti-Myc) with telomeres (TTAGGG FISH) in U2OS after 3 days of DOX induction. Scale bars, 10 μm.

(C) Representative image and quantification of H3 and H3K9me3 chromatin immunoprecipitation HeLa LT expressing the indicated constructs. Data represent mean ± SEM of $n = 3$ biological replicates.

(D and E) Western blot showing ATRX, Myc (TRF1-fusion constructs), and H3K9me3 in HeLa LT (D) and HeLa ST (E), parental and ATRX-KO clones expressing the indicated constructs.

*(legend continued on next page)*

interesting questions regarding how epigenetic regulation of telomeres may or may not contribute to ALT in these experimental systems. In light of our findings, these observations could indicate that the specific paradoxical chromatin environment observed at ALT+ telomeres reduced nucleosome density, combined with enrichment of heterochromatin-associated features and factors, may be critical to facilitate productive ALT-mediated telomere elongation.

Broadly, our findings position heterochromatin-driven telomere organization as a facilitating step in ALT rather than a direct trigger of recombination. While enrichment of telomeric H3K9me3 and HP1α promotes telomere clustering and *de novo* PML-NB assembly, recombination-associated features emerge only in specific cellular contexts, and even in these contexts, productive telomere extension was not evident. This separation suggests that additional factors or cellular states are required to enable recombination downstream of heterochromatin-mediated compartmentalization and to couple these events to stable telomere extension. Defining the determinants that convert heterochromatin-driven organization into productive ALT activity will be an important direction for future studies.

### Limitations of the study

Several limitations should be considered when interpreting these findings. Our approach relies on TRF1 fusion proteins involving overexpression, which may not fully recapitulate the physiological heterochromatin dynamics at telomeres, and notably, TRF1 overexpression alone reduced baseline APB levels and telomere clustering. The phenotypes observed with TRF1-HP1α exhibited substantial cell-to-cell heterogeneity, with some cells displaying telomere entanglements while others showed ultra-bright APBs, and the determinants underlying this variability remain unclear. Furthermore, our use of indirect biomarkers such as C-circles and G2-phase EdU incorporation provides evidence consistent with telomeric recombination but does not directly measure homology-directed repair events or template-driven synthesis at telomeres. Finally, the context-dependency of our findings, particularly the differences between cell lines with long vs. short telomeres and between ALT-positive and non-ALT backgrounds, suggests that cell-type-specific factors influence the capacity of heterochromatin to promote recombination-associated phenotypes, though these factors remain to be identified.

## RESOURCE AVAILABILITY

### Lead contact

Request for further information and resources should be directed to the lead contact, Nausica Arnoult (nausica.arnoult@colorado.edu).

### Materials availability

Materials used in this study are available upon reasonable request.

### Data and code availability

- Data reported in this paper will be shared by the lead contact upon request.
- This paper does not report original code.
- Any additional information required to reanalyze the data reported in this paper is available from the lead contact upon request.

## ACKNOWLEDGMENTS

We thank Dr. James Orth and the MCDB Light Microscopy core facility; the MCDB Flow Cytometry facility; as well as Joseph Dragavon, Erin Richards, and the BioFrontiers Advanced Light Microscopy Core. The use of the microscopy core facilities was enabled by the CU Boulder Core Facility Voucher program ID: CUBoulder_FY26_VP04. We thank Thomas Cech and all the members of the Arnoult lab for their input on the manuscript. This work was funded by the NIH (R35GM143108 to N.A. and T32GM142607 to E.R.T.), the NSF (GRFP DGE2040434 to E.R.T.), the Boettcher Foundation (AWD-21-02-0209 to N.A.), and the V Foundation for Cancer Research (V2021-031 to N.A.). G.W. is supported by the Howard Hughes Medical Institute. M.V., M.M., M.R., and A.D. are funded by FNRS, Belgium and Télévie, Belgium.

## AUTHOR CONTRIBUTIONS

Data were generated by B.P. III, E.R.T., M.V., G.W., S.S., D.M., L.W., S.B., M.M., and M.R. Analyses were performed by B.P. III, E.R.T., M.V., G.W., and N.A. Manuscript was written by E.R.T. and N.A. and was reviewed by all authors. Funding for this project was acquired by N.A. and A.D.

## DECLARATION OF INTERESTS

The authors declare no competing interests.

## DECLARATION OF GENERATIVE AI AND AI-ASSISTED TECHNOLOGIES IN THE WRITING PROCESS

During the preparation of this work, the authors used OpenAI in order to help improve the language and readability of certain sentences. After using this tool/service, the authors reviewed and edited the content as needed and take full responsibility for the content of the publication.

## STAR★METHODS

Detailed methods are provided in the online version of this paper and include the following:

- KEY RESOURCES TABLE
- EXPERIMENTAL MODEL AND SUBJECT DETAILS
  - Cell lines and cell culture
- METHOD DETAILS
  - Plasmids and cell transductions and transfections
  - Western blots
  - Immunofluorescence and immunofluorescence-FISH
  - Flow cytometry for fusion construct expression
  - C-circle assay

(F) Quantification of telomere-PML colocalized foci (TPF) in the indicated cell lines. Data represent mean ± SEM of all cells from 3 independent biological replicates. *n* (number of cells analyzed, in the order presented in the figure) = 124, 126, 125, 121, 117, 102, 135, 107, 99, 115, 128, and 128.
(G) Western blot showing the expression of TRF1-KDM4D in U2OS.
(H) Representative images of IF-FISH showing colocalization of the fusion-protein (anti-Myc) and PML bodies (PML) with telomeres (TTAGGG) in U2OS expressing the indicated constructs after 3 days of DOX induction. Scale bars, 10 μm.
(I–L) Quantification of (H). Number of telomeric foci per cell (J), number of TPF per cell (K), mean PML foci area (J), and number of PML foci per cell (K). Data represent mean ± SEM of all cells from 3 independent biological replicates. *n* (number of cells analyzed) = 102 (Ø), 113 (TRF1), and 114 (TRF1-KDM4D).
Statistical analyses: for (C), Welch's *t* test. For (F and I–L), ordinary one-way ANOVA. $^{*}p < 0.05$, $^{**}p < 0.01$, $^{***}p < 0.001$, and $^{****}p < 0.0001$. ns, non-significant.

- Slot blot hybridization
- Mitotic DNA synthesis
- G2 EdU incorporation FISH
- Chromatin immunoprecipitation
- Cell growth assay
- Electroporation to generate KO cells

- QUANTIFICATIONS AND STATISTICAL ANALYSES

## SUPPLEMENTAL INFORMATION

Supplemental information can be found online at https://doi.org/10.1016/j.celrep.2026.117004.

Received: July 15, 2025
Revised: December 15, 2025
Accepted: January 22, 2026
Published: February 18, 2026

## REFERENCES

1. Heaphy, C.M., de Wilde, R.F., Jiao, Y., Klein, A.P., Edil, B.H., Shi, C., Bettegowda, C., Rodriguez, F.J., Eberhart, C.G., Hebbar, S., et al. (2011). Altered telomeres in tumors with ATRX and DAXX mutations. Science *333*, 425. https://doi.org/10.1126/science.1207313.
2. Min, J., Wright, W.E., and Shay, J.W. (2017). Alternative Lengthening of Telomeres Mediated by Mitotic DNA Synthesis Engages Break-Induced Replication Processes. Mol. Cell Biol. *37*, e00226-17. https://doi.org/10.1128/MCB.00226-17.
3. Dunham, M.A., Neumann, A.A., Fasching, C.L., and Reddel, R.R. (2000). Telomere maintenance by recombination in human cells. Nat. Genet. *26*, 447–450.
4. Dilley, R.L., Verma, P., Cho, N.W., Winters, H.D., Wondisford, A.R., and Greenberg, R.A. (2016). Break-induced telomere synthesis underlies alternative telomere maintenance. Nature *539*, 54–58. https://doi.org/10.1038/nature20099.
5. Yeager, T.R., Neumann, A.A., Englezou, A., Huschtscha, L.I., Noble, J.R., and Reddel, R.R. (1999). Telomerase-negative immortalized human cells contain a novel type of promyelocytic leukemia (PML) body. Cancer Res. *59*, 4175–4179.
6. Zhang, J.M., and Zou, L. (2020). Alternative lengthening of telomeres: from molecular mechanisms to therapeutic outlooks. Cell Biosci. *10*, 30. https://doi.org/10.1186/s13578-020-00391-6.
7. Lovejoy, C.A., Li, W., Reisenweber, S., Thongthip, S., Bruno, J., de Lange, T., De, S., Petrini, J.H.J., Sung, P.A., Jasin, M., et al. (2012). Loss of ATRX, genome instability, and an altered DNA damage response are hallmarks of the alternative lengthening of telomeres pathway. PLoS Genet. *8*, e1002772. https://doi.org/10.1371/journal.pgen.1002772.
8. Napier, C.E., Huschtscha, L.I., Harvey, A., Bower, K., Noble, J.R., Hendrickson, E.A., and Reddel, R.R. (2015). ATRX represses alternative lengthening of telomeres. Oncotarget *6*, 16543–16558. https://doi.org/10.18632/oncotarget.3846.
9. Schoeftner, S., and Blasco, M. (2009). A 'higher order' of telomere regulation: telomere heterochromatin and telomeric RNAs. EMBO J. *28*, 2323–2336. https://doi.org/10.1038/emboj.2009.197.
10. Bettin, N., Vaurs, M., and Decottignies, A. (2025). Epigenetics of Human Telomeres. Cold Spring Harb. Perspect. Biol. *17*, a041706. https://doi.org/10.1101/cshperspect.a041706.
11. Episkopou, H., Draskovic, I., Van Beneden, A., Tilman, G., Mattiussi, M., Gobin, M., Arnoult, N., Londoño-Vallejo, A., and Decottignies, A. (2014). Alternative Lengthening of Telomeres is characterized by reduced compaction of telomeric chromatin. Nucleic Acids Res. *42*, 4391–4405. https://doi.org/10.1093/nar/gku114.
12. Azzalin, C.M., Reichenbach, P., Khoriauli, L., Giulotto, E., and Lingner, J. (2007). Telomeric repeat containing RNA and RNA surveillance factors at mammalian chromosome ends. Science *318*, 798–801.
13. Li, F., Deng, Z., Zhang, L., Wu, C., Jin, Y., Hwang, I., Vladimirova, O., Xu, L., Yang, L., Lu, B., et al. (2019). ATRX loss induces telomere dysfunction and necessitates induction of alternative lengthening of telomeres during human cell immortalization. EMBO J. *38*, e96659. https://doi.org/10.15252/embj.201796659.
14. Tilman, G., Loriot, A., Van Beneden, A., Arnoult, N., Londoño-Vallejo, J.A., De Smet, C., and Decottignies, A. (2009). Subtelomeric DNA hypomethylation is not required for telomeric sister chromatid exchanges in ALT cells. Oncogene *28*, 1682–1693. https://doi.org/10.1038/onc.2009.23.
15. Gauchier, M., Kan, S., Barral, A., Sauzet, S., Agirre, E., Bonnell, E., Saksouk, N., Barth, T.K., Ide, S., Urbach, S., et al. (2019). SETDB1-dependent heterochromatin stimulates alternative lengthening of telomeres. Sci. Adv. *5*, eaav3673. https://doi.org/10.1126/sciadv.aav3673.
16. O'Sullivan, R.J., Arnoult, N., Lackner, D.H., Oganesian, L., Haggblom, C., Corpet, A., Almouzni, G., and Karlseder, J. (2014). Rapid induction of alternative lengthening of telomeres by depletion of the histone chaperone ASF1. Nat. Struct. Mol. Biol. *21*, 167–174. https://doi.org/10.1038/nsmb.2754.
17. Hartlieb, S.A., Sieverling, L., Nadler-Holly, M., Ziehm, M., Toprak, U.H., Herrmann, C., Ishaque, N., Okonechnikov, K., Gartlgruber, M., Park, Y.G., et al. (2021). Alternative lengthening of telomeres in childhood neuroblastoma from genome to proteome. Nat. Commun. *12*, 1269. https://doi.org/10.1038/s41467-021-21247-8.
18. Shi, G., Hu, Y., Zhu, X., Jiang, Y., Pang, J., Wang, C., Huang, W., Zhao, Y., Ma, W., Liu, D., et al. (2020). A critical role of telomere chromatin compaction in ALT tumor cell growth. Nucleic Acids Res. *48*, 6019–6031. https://doi.org/10.1093/nar/gkaa224.
19. Wang, C., Songyang, Z., and Huang, Y. (2021). TRIM28 inhibits alternative lengthening of telomere phenotypes by protecting SETDB1 from degradation. Cell Biosci. *11*, 149. https://doi.org/10.1186/s13578-021-00660-y.
20. Dejardin, J., and Kingston, R.E. (2009). Purification of proteins associated with specific genomic Loci. Cell *136*, 175–186, S0092-8674(08)01520-1 [pii]. https://doi.org/10.1016/j.cell.2008.11.045.
21. Jiang, W.Q., Nguyen, A., Cao, Y., Chang, A.C.M., and Reddel, R.R. (2011). HP1-mediated formation of alternative lengthening of telomeres-associated PML bodies requires HIRA but not ASF1a. PLoS One *6*, e17036. https://doi.org/10.1371/journal.pone.0017036.
22. Wang, B., Kou, H., Wang, Y., Zhang, Q., Jiang, D., Wang, J., Zhao, Z., Zhou, Y., Zhang, M., Sui, L., et al. (2024). LAP2alpha orchestrates alternative lengthening of telomeres suppression through telomeric heterochromatin regulation with HDAC1: unveiling a potential therapeutic target. Cell Death Dis. *15*, 761. https://doi.org/10.1038/s41419-024-07116-4.
23. Witzgall, R., O'Leary, E., Leaf, A., Onaldi, D., and Bonventre, J.V. (1994). The Kruppel-associated box-A (KRAB-A) domain of zinc finger proteins mediates transcriptional repression. Proc. Natl. Acad. Sci. USA *91*, 4514–4518. https://doi.org/10.1073/pnas.91.10.4514.
24. Cho, N.W., Dilley, R.L., Lampson, M.A., and Greenberg, R.A. (2014). Interchromosomal homology searches drive directional ALT telomere movement and synapsis. Cell *159*, 108–121. https://doi.org/10.1016/j.cell.2014.08.030.
25. Garcia-Exposito, L., Bournique, E., Bergoglio, V., Bose, A., Barroso-Gonzalez, J., Zhang, S., Roncaioli, J.L., Lee, M., Wallace, C.T., Watkins, S.C., et al. (2016). Proteomic Profiling Reveals a Specific Role for Translesion DNA Polymerase eta in the Alternative Lengthening of Telomeres. Cell Rep. *17*, 1858–1871. https://doi.org/10.1016/j.celrep.2016.10.048.
26. Gaela, V.M., Hsia, H.Y., Joseph, N.A., Tzeng, W.Y., Ting, P.C., Shen, Y.L., Tsai, C.T., Boudier, T., and Chen, L.Y. (2024). Orphan nuclear receptors-induced ALT-associated PML bodies are targets for ALT inhibition. Nucleic Acids Res. *52*, 6472–6489. https://doi.org/10.1093/nar/gkae389.

27. Chow, T.T., Shi, X., Wei, J.H., Guan, J., Stadler, G., Huang, B., and Blackburn, E.H. (2018). Local enrichment of HP1alpha at telomeres alters their structure and regulation of telomere protection. Nat. Commun. *9*, 3583. https://doi.org/10.1038/s41467-018-05840-y.

28. Schultz, D.C., Ayyanathan, K., Negorev, D., Maul, G.G., and Rauscher, F.J., 3rd. (2002). SETDB1: a novel KAP-1-associated histone H3, lysine 9-specific methyltransferase that contributes to HP1-mediated silencing of euchromatic genes by KRAB zinc-finger proteins. Genes Dev. *16*, 919–932. https://doi.org/10.1101/gad.973302.

29. Sfeir, A., Kosiyatrakul, S.T., Hockemeyer, D., MacRae, S.L., Karlseder, J., Schildkraut, C.L., and de Lange, T. (2009). Mammalian telomeres resemble fragile sites and require TRF1 for efficient replication. Cell *138*, 90–103, S0092-8674(09)00721-1 [pii]. https://doi.org/10.1016/j.cell.2009.06.021.

30. Vaurs, M., Claude, E., Zanella, E., Rodrigues, J., Nassour, J., Karlseder, J., Azzalin, C.M., Doksani, Y., and Decottignies, A. (2025). TRF1 relies on fork reversal to prevent fragility at human telomeres. Nat. Commun. *16*, 6439. https://doi.org/10.1038/s41467-025-61828-5.

31. Lu, R., and Pickett, H.A. (2022). Telomeric replication stress: the beginning and the end for alternative lengthening of telomeres cancers. Open Biol. *12*, 220011. https://doi.org/10.1098/rsob.220011.

32. Bai, G., Endres, T., Kuhbacher, U., Mengoli, V., Greer, B.H., Peacock, E.M., Newton, M.D., Stanage, T., Dello Stritto, M.R., Lungu, R., et al. (2024). HLTF resolves G4s and promotes G4-induced replication fork slowing to maintain genome stability. Mol Cell *84*, 3044-3060 e3011. https://doi.org/10.1016/j.molcel.2024.07.018.

33. Bryan, T.M., Englezou, A., Dalla-Pozza, L., Dunham, M.A., and Reddel, R.R. (1997). Evidence for an alternative mechanism for maintaining telomere length in human tumors and tumor-derived cell lines. Nat. Med. *3*, 1271–1274.

34. Bryan, T.M., Englezou, A., Gupta, J., Bacchetti, S., and Reddel, R.R. (1995). Telomere elongation in immortal human cells without detectable telomerase activity. EMBO J. *14*, 4240–4248.

35. Henson, J.D., Cao, Y., Huschtscha, L.I., Chang, A.C., Au, A.Y.M., Pickett, H.A., and Reddel, R.R. (2009). DNA C-circles are specific and quantifiable markers of alternative-lengthening-of-telomeres activity. Nat. Biotechnol. *27*, 1181–1185, nbt.1587 [pii]. https://doi.org/10.1038/nbt.1587.

36. Bannister, A.J., Zegerman, P., Partridge, J.F., Miska, E.A., Thomas, J.O., Allshire, R.C., and Kouzarides, T. (2001). Selective recognition of methylated lysine 9 on histone H3 by the HP1 chromo domain. Nature *410*, 120–124.

37. Loyola, A., Tagami, H., Bonaldi, T., Roche, D., Quivy, J.P., Imhof, A., Nakatani, Y., Dent, S.Y.R., and Almouzni, G. (2009). The HP1alpha-CAF1-SetDB1-containing complex provides H3K9me1 for Suv39-mediated K9me3 in pericentric heterochromatin. EMBO Rep. *10*, 769–775, embor200990 [pii]. https://doi.org/10.1038/embor.2009.90.

38. Canzio, D., Chang, E.Y., Shankar, S., Kuchenbecker, K.M., Simon, M.D., Madhani, H.D., Narlikar, G.J., and Al-Sady, B. (2011). Chromodomain-mediated oligomerization of HP1 suggests a nucleosome-bridging mechanism for heterochromatin assembly. Mol. Cell *41*, 67–81. https://doi.org/10.1016/j.molcel.2010.12.016.

39. Nielsen, A.L., Oulad-Abdelghani, M., Ortiz, J.A., Remboutsika, E., Chambon, P., and Losson, R. (2001). Heterochromatin formation in mammalian cells: interaction between histones and HP1 proteins. Mol. Cell *7*, 729–739. https://doi.org/10.1016/s1097-2765(01)00218-0.

40. Pan, X., Chen, Y., Biju, B., Ahmed, N., Kong, J., Goldenberg, M., Huang, J., Mohan, N., Klosek, S., Parsa, K., et al. (2019). FANCM suppresses DNA replication stress at ALT telomeres by disrupting TERRA R-loops. Sci. Rep. *9*, 19110. https://doi.org/10.1038/s41598-019-55537-5.

41. Silva, B., Pentz, R., Figueira, A.M., Arora, R., Lee, Y.W., Hodson, C., Wischnewski, H., Deans, A.J., and Azzalin, C.M. (2019). FANCM limits ALT activity by restricting telomeric replication stress induced by deregulated BLM and R-loops. Nat. Commun. *10*, 2253. https://doi.org/10.1038/s41467-019-10179-z.

42. Fernandez-Casanas, M., and Chan, K.L. (2018). The Unresolved Problem of DNA Bridging. Genes *9*, 623. https://doi.org/10.3390/genes9120623.

43. Jiang, H., and Chan, Y.W. (2024). Chromatin bridges: stochastic breakage or regulated resolution? Trends Genet. *40*, 69–82. https://doi.org/10.1016/j.tig.2023.10.004.

44. Meyer-Nava, S., Nieto-Caballero, V.E., Zurita, M., and Valadez-Graham, V. (2020). Insights into HP1a-Chromatin Interactions. Cells *9*, 1866. https://doi.org/10.3390/cells9081866.

45. Pickett, H.A., Cesare, A.J., Johnston, R.L., Neumann, A.A., and Reddel, R.R. (2009). Control of telomere length by a trimming mechanism that involves generation of t-circles. EMBO J. *28*, 799–809.

46. Arnoult, N., Van Beneden, A., and Decottignies, A. (2012). Telomere length regulates TERRA levels through increased trimethylation of telomeric H3K9 and HP1alpha. Nat. Struct. Mol. Biol. *19*, 948–956. https://doi.org/10.1038/nsmb.2364.

47. van Steensel, B., Smogorzewska, A., and de Lange, T. (1998). TRF2 protects human telomeres from end-to-end fusions. Cell *92*, 401–413.

48. Loe, T.K., Li, J.S.Z., Zhang, Y., Azeroglu, B., Boddy, M.N., and Denchi, E.L. (2020). Telomere length heterogeneity in ALT cells is maintained by PML-dependent localization of the BTR complex to telomeres. Genes Dev. *34*, 650–662. https://doi.org/10.1101/gad.333963.119.

49. Nozawa, R.-S., Nagao, K., Masuda, H.-T., Iwasaki, O., Hirota, T., Nozaki, N., Kimura, H., and Obuse, C. (2010). Human POGZ modulates dissociation of HP1alpha from mitotic chromosome arms through Aurora B activation. Nat. Cell Biol. *12*, 719–727. https://doi.org/10.1038/ncb2075.

50. Zhao, R., Xu, M., Yu, X., Wondisford, A.R., Lackner, R.M., Salsman, J., Dellaire, G., Chenoweth, D.M., O'Sullivan, R.J., Zhao, X., and Zhang, H. (2024). SUMO promotes DNA repair protein collaboration to support alternative telomere lengthening in the absence of PML. Genes Dev. *38*, 614–630. https://doi.org/10.1101/gad.351667.124.

51. Draskovic, I., Arnoult, N., Steiner, V., Bacchetti, S., Lomonte, P., and Londoño-Vallejo, A. (2009). Probing PML body function in ALT cells reveals spatiotemporal requirements for telomere recombination. Proc. Natl. Acad. Sci. USA *106*, 15726–15731, AuthorAnonymous, 0907689106 [pii]. https://doi.org/10.1073/pnas.0907689106.

52. Lisaingo, K., Uringa, E.J., and Lansdorp, P.M. (2014). Resolution of telomere associations by TRF1 cleavage in mouse embryonic stem cells. Mol. Biol. Cell *25*, 1958–1968. https://doi.org/10.1091/mbc.E13-10-0564.

53. Seeler, J.S., Marchio, A., Sitterlin, D., Transy, C., and Dejean, A. (1998). Interaction of SP100 with HP1 proteins: a link between the promyelocytic leukemia-associated nuclear bodies and the chromatin compartment. Proc. Natl. Acad. Sci. USA *95*, 7316–7321. https://doi.org/10.1073/pnas.95.13.7316.

54. Jiang, W.Q., Zhong, Z.H., Henson, J.D., Neumann, A.A., Chang, A.C.M., and Reddel, R.R. (2005). Suppression of alternative lengthening of telomeres by Sp100-mediated sequestration of the MRE11/RAD50/NBS1 complex. Mol. Cell Biol. *25*, 2708–2721, 25/7/2708 [pii]. https://doi.org/10.1128/MCB.25.7.2708-2721.2005.

55. Boisvert, F.M., van Koningsbruggen, S., Navascués, J., and Lamond, A.I. (2007). The multifunctional nucleolus. Nat. Rev. Mol. Cell Biol. *8*, 574–585. https://doi.org/10.1038/nrm2184.

56. Lallemand-Breitenbach, V., and de Thé, H. (2018). PML nuclear bodies: from architecture to function. Curr. Opin. Cell Biol. *52*, 154–161. https://doi.org/10.1016/j.ceb.2018.03.011.

57. Sahin, U., Ferhi, O., Jeanne, M., Benhenda, S., Berthier, C., Jollivet, F., Niwa-Kawakita, M., Faklaris, O., Setterblad, N., de Thé, H., and Lallemand-Breitenbach, V. (2014). Oxidative stress-induced assembly of PML nuclear bodies controls sumoylation of partner proteins. J. Cell Biol. *204*, 931–945. https://doi.org/10.1083/jcb.201305148.

58. Grotzinger, T., Jensen, K., and Will, H. (1996). The interferon (IFN)-stimulated gene Sp100 promoter contains an IFN-gamma activation site and an imperfect IFN-stimulated response element which mediate type I IFN

inducibility. J. Biol. Chem. *271*, 25253–25260. https://doi.org/10.1074/jbc.271.41.25253.

59. Everett, R.D., and Chelbi-Alix, M.K. (2007). PML and PML nuclear bodies: implications in antiviral defence. Biochimie *89*, 819–830. https://doi.org/10.1016/j.biochi.2007.01.004.
60. Kleijwegt, C., Bressac, F., Seurre, C., Bouchereau, W., Cohen, C., Texier, P., Simonet, T., Schaeffer, L., Lomonte, P., and Corpet, A. (2023). Interplay between PML NBs and HIRA for H3.3 dynamics following type I interferon stimulus. eLife *12*, e80156. https://doi.org/10.7554/eLife.80156.
61. Hsu, J.K., Lin, T., and Tsai, R.Y.L. (2012). Nucleostemin prevents telomere damage by promoting PML-IV recruitment to SUMOylated TRF1. J. Cell Biol. *197*, 613–624. https://doi.org/10.1083/jcb.201109038.
62. Berry, W.L., and Janknecht, R. (2013). KDM4/JMJD2 histone demethylases: epigenetic regulators in cancer cells. Cancer Res. *73*, 2936–2942. https://doi.org/10.1158/0008-5472.CAN-12-4300.
63. Hyun, K., Jeon, J., Park, K., and Kim, J. (2017). Writing, erasing and reading histone lysine methylations. Exp. Mol. Med. *49*, e324. https://doi.org/10.1038/emm.2017.11.
64. Udugama, M., Hii, L., Garvie, A., Cervini, M., Vinod, B., Chan, F.L., Das, P.P., Mann, J.R., Collas, P., Voon, H.P.J., and Wong, L.H. (2021). Mutations inhibiting KDM4B drive ALT activation in ATRX-mutated glioblastomas. Nat. Commun. *12*, 2584. https://doi.org/10.1038/s41467-021-22543-z.
65. Lu, R., Nelson, C.B., Rogers, S., Cesare, A.J., Sobinoff, A.P., and Pickett, H.A. (2024). Distinct modes of telomere synthesis and extension contribute to Alternative Lengthening of Telomeres. iScience *27*, 108655. https://doi.org/10.1016/j.isci.2023.108655.
66. Segura-Bayona, S., Villamor-Payà, M., Attolini, C.S.O., Koenig, L.M., Sanchiz-Calvo, M., Boulton, S.J., and Stracker, T.H. (2020). Tousled-Like Kinases Suppress Innate Immune Signaling Triggered by Alternative Lengthening of Telomeres. Cell Rep. *32*, 107983. https://doi.org/10.1016/j.celrep.2020.107983.
67. Guan, B., Wang, T.L., and Shih, I.M. (2011). ARID1A, a factor that promotes formation of SWI/SNF-mediated chromatin remodeling, is a tumor suppressor in gynecologic cancers. Cancer Res. *71*, 6718–6727. https://doi.org/10.1158/0008-5472.CAN-11-1562.
68. Vernier, M., Bourdeau, V., Gaumont-Leclerc, M.F., Moiseeva, O., Bégin, V., Saad, F., Mes-Masson, A.M., and Ferbeyre, G. (2011). Regulation of E2Fs and senescence by PML nuclear bodies. Genes Dev. *25*, 41–50. https://doi.org/10.1101/gad.1975111.
69. Cheutin, T., McNairn, A.J., Jenuwein, T., Gilbert, D.M., Singh, P.B., and Misteli, T. (2003). Maintenance of stable heterochromatin domains by dynamic HP1 binding. Science *299*, 721–725. https://doi.org/10.1126/science.1078572.
70. Wu, G., Taylor, E., Youmans, D.T., Arnoult, N., and Cech, T.R. (2025). Rapid dynamics allow the low-abundance RTEL1 helicase to promote telomere replication. Nucleic Acids Res. *53*, gkaf177. https://doi.org/10.1093/nar/gkaf177.

## STAR★METHODS

### KEY RESOURCES TABLE

| REAGENT or RESOURCE | SOURCE | IDENTIFIER |
|---|---|---|
| Antibodies | | |
| PML antibody | Bethyl Laboratories | Cat# A301-167A; RRID:AB_873108 |
| PML antibody | Santa Cruz Biotechnology | Cat# sc-966; RRID:AB_628162 |
| SP100 antibody | Abcam | Cat# ab167605; RRID: AB_3716604 |
| ATRX antibody | Cell Signaling Technology | Cat# 10321; RRID: AB_2940903 |
| SETDB1 antibody | Abcam | Cat# ab107225; RRID: AB_10861045 |
| DAXX antibody | Cell Signaling Technology | Cat# 4533; RRID: AB_2088778 |
| HP1α antibody | Abcam | Cat# ab77256; RRID: AB_1523784 |
| Myc-tag antibody | Cell Signaling Technology | Cat# 2276; RRID: AB_331783 |
| β-Actin antibody | Cell Signaling Technology | Cat# 8457; RRID: AB_10950489 |
| H3K9me3 antibody | Abcam | Cat# ab8898; RRID: AB_306848 |
| Histone H3 antibody | Abcam | Cat# ab1791; RRID: AB_302613 |
| IgG control antibody | Abcam | Cat# ab37415 |
| TRF2 antibody | Novus Biologicals | Cat# NB110-57130; RRID: AB_844199 |
| BLM antibody | Bethyl Laboratories, Thermo Fisher | Cat# A300-110A; RRID: AB_2779016 |
| Anti-Digoxigenin-AP, Fab fragments | Roche | Cat# 11093274910; RRID: AB_514497 |
| Anti-mouse HRP | Cell Signaling Technology | Cat# 7076; RRID: AB_330924 |
| Anti-rabbit HRP | Cell Signaling Technology | Cat# 7074; RRID: AB_2099233 |
| Alexa Fluor 568 goat anti-rabbit IgG | Invitrogen | Cat# A11036; RRID: AB_10563566 |
| Alexa Fluor 568 goat anti-mouse IgG | Invitrogen | Cat# A11031; RRID: AB_144696 |
| Alexa Fluor 568 goat anti-rabbit IgG | Invitrogen | Cat# A11008; RRID: AB_143165 |
| Alexa Fluor 488 goat anti-mouse IgG | Invitrogen | Cat# A11001; RRID: AB_2534069 |
| Alexa Fluor 647 goat anti-mouse IgG | Invitrogen | Cat# A21236; RRID: AB_2535805 |
| Bacterial and virus strains | | |
| NEB Stable | New England Biolabs | C3040 |
| Chemicals, peptides, and recombinant proteins | | |
| Blasticidin | RPI | B12200–0.05 |
| Polybrene | Santa Cruz Biotechnology | Cat# sc-134220 |
| DMEM | Corning | Cat# 10-013CV |
| Carbenecillin | IBI Scientific 3P | IB02025 |
| Colcemid | Gibco KaryoMAX | 15212–012 |
| Doxycycline | TCI | D4116 |
| RO3306 CDK1 inhibitor | Millipore Sigma | Cat# SML0569 |
| Fluoroshield with DAPI | Sigma-Aldrich | F6057 |
| HEPES | GIBCO | 15630080 |
| MEM Nonessential Amino Acids | Corning | 25-025CI |
| Penicilin/Streptomycin | Lonza | 09-757F |
| Puromycin | Alfa Aesar | 61278-MC |
| NEBNext Ultra II Q5 Master Mix | NEB | M0544X |
| Triton X- | MP Biomedicals | 9002-93-1 |
| PEI Max | Polysciences Inc. | 24765–1 |
| HyClone Cosmic Calf Serum | Cytiva | SH30087.04 |
| Thymidine | Millipore Sigma | Cat# T9250 |
| SUMO inhibitor (SUMOi) | Selleck Chemical | Cat# S8697 |
| Opti-MEM I | Gibco | Cat# 31985-070 |

(*Continued on next page*)

*Continued*

| REAGENT or RESOURCE | SOURCE | IDENTIFIER |
|---|---|---|
| Lipofectamine RNAiMAX | Thermo Fisher Scientific | Cat# 13778030 |
| Lipofectamine 3000 | Thermo Fisher Scientific | Cat# L3000015 |
| HMW Poly(I:C) | InvivoGen | Cat# tlrl-pic |
| Protease | QIAGEN | Cat# 19157 |
| Benzonase Nuclease | EMD Millipore | Cat# 70746-3 |
| Formamide | Millipore Sigma | Cat# S4117 |
| Blocking reagent | Roche | Cat# 11096176001 |
| Phenol/Chloroform/Isoamyl alcohol (25:24:1) | Acros Organics | Cat# 32711500 |
| Chloroform | Fisher Chemical | Cat# C574-1 |
| 100% Ethanol | Decon Laboratories, Inc. | Cat# 2701 |
| Sodium Acetate | VWR | Cat# 0602-500G |
| HinfI restriction enzyme | New England Biolabs | Cat# R0155L |
| RsaI restriction enzyme | New England Biolabs | Cat# R0167 |
| Φ29 Reaction Buffer | New England Biolabs | Cat# B0269S |
| dNTP mix | Qiagen | Cat# 201913 |
| Φ29 DNA Polymerase | New England Biolabs | Cat# M0629L |
| CDP-Star | Roche | Cat# 11759051001 |
| Pepsin | Fisher Scientific | Cat# A104-500 |
| Paraformaldehyde, 16% w/v aq soln., methanol free | Thermo Scientific | Cat. No: 043368.9 |
| RNase A | Thermo Scientific | Ref# EN0531 |
| Protein A/G Magnetic Beads | Thermo Scientific | Cat# 88802 |
| Protease inhibitor cocktail | Roche | Cat# 05892791001 |
| ChIP protease inhibitor mix | Diagenode | Cat# C12010011 |
| Nucleofection buffer | MaxCyte | Cat# EPB-1 |
| Cas9 protein | IDT | Cat# 1081060 |
| Neomycin | Thermo Scientific | J62671.03 |
| **Critical commercial assays** | | |
| BCA Protein Assay | ThermoFischer | 23227 |
| DIG Oligonucleotide 3′ End Labeling Kit, 2ND generation | Roche | Cat# 03353575910 |
| Qubit High Sensitivity dsDNA Kit | Invitrogen | Q32851 |
| Click-iT EdU Cell Proliferation Kit for Imaging | Thermo Fisher Scientific | Cat# C10340 |
| Qiagen DNA Purification Kit | Qiagen | Cat# 28106 |
| DNA Clean and Concentrator 5-G | Zymo Research | D4013 |
| Infusion | Takara | 638948 |
| Zymoclean Gel DNA Recovery Kit | Zymo Research | D4001 |
| Super Signal West Dura | Genesee Scientific | 20–301 |
| Super Signal West Femto | Genesee Scientific | 20–302 |
| Amersham Hybond P 0.2μm PVDF | Cytiva | 10600021 |
| Bolt 4%–12% Bis-Tris Plus gels | Invitrogen | NW04120 |
| Nucleofection Buffer | MaxCyte | EPB-1 |
| Electroporation cuvette | MaxCyte | SOC-25x3 |
| **Experimental models: Cell lines** | | |
| U2-OS | ATCC | HTB-96 |
| Lenti-X 293-T | Takara | 632180 |
| HeLa ST | Karlseder lab | – |
| HeLa LT (HeLa 1.2.11) | Karlseder lab | – |
| WI-38 VA13 | Karlseder lab | – |
| Saos-2 | ATCC | HTB-85 |
| IMR90 E6E7 | Nassour lab | – |

(*Continued on next page*)

*Continued*

| REAGENT or RESOURCE | SOURCE | IDENTIFIER |
|---|---|---|
| **Oligonucleotides** | | |
| TelC-FAM | PNA Bio Inc. | F1001 |
| CENPB-Cy3 | PNA Bio Inc. | F3002 |
| Alexa 488-OO-(CCCTAA)3 PNA telomere probe | PNA Bio Inc. | Cat# F1001 |
| ON-TARGETplus Non-targeting siRNA | Horizon Discovery (Dharmacon) SmartPOOL | UGGUUUACAUGUCGACUAA<br>UGGUUUACAUGUUGUGUGA<br>UGGUUUACAUGUUUUCUGA<br>UGGUUUACAUGUUUUCCUA |
| ON-TARGETplus SP100 siRNA | Horizon Discovery (Dharmacon) SmartPOOL | GAAGUGAGCCUGUGAUCAA<br>AGGCAUAGAUCUAAAGUAA<br>UACCAGAGCCCAUGGAUUU<br>GAAGGGCACUCUAUAUAAG |
| ON-TARGETplus ATRX siRNA | Horizon Discovery (Dharmacon) SmartPOOL | GAUGUUAGCUGGAUGUGUU<br>AGUCAUAGAUGCUAAGUUU<br>GCUUGAGGUUUCUGAAUUA<br>GUACAGGCGUUAGCAUUAA |
| ON-TARGETplus DAXX siRNA | Horizon Discovery (Dharmacon) SmartPOOL | CAGCCAAGCUCUAUGUCUA<br>GAGGUUAACAGGCGCAUUG<br>GCAAAACAAAGGACGCAUA<br>GGAGUUGGAUCUCUCAGAA |
| ON-TARGETplus SETDB1 siRNA | Horizon Discovery (Dharmacon) SmartPOOL | AAGAUGGGCUUUCAUGUUA<br>GAACUAAGACUUGGCACAA<br>GGGAUCAACCAGACAUAUA<br>GAGCGCACCUGUUCGUAAG |
| HP1α 3′UTR siRNA | Lou et al. 2024 | GUUGGAAUCUUACUAGUC |
| HP1α 3′UTR siRNA | Lou et al. 2024 | CUUCUGUAAAGUGAUAUC |
| Telomere probe (CCCTAA)4 | IDT | CCCTAAC CCTAAC CCTAAC CCTAA |
| Alu probe | IDT | GTAATCCCAGCACTTTGG |
| sgRNA targeting ATRX | Synthego | AUGAUUUAAAGACUCAGGCG |
| sgRNA targeting PML | Synthego | AGACCUCACUUCCUAUGACG |
| **Recombinant DNA** | | |
| pLentiPuro-Transfer | Guan et al.[67] | Addgene #39481 |
| pLIX_403 doxycycline-inducible lentiviral backbone | Gift from David Root | Addgene #41395 |
| PML-IV expression plasmid | Vernier et al.[68] | Plasmid #62804 |
| HP1α expression plasmid | Cheutin et al.[69] | Plasmid #17652 |
| **Software and algorithms** | | |
| GraphPad Prism9 | GraphPad | 9.0.1 |
| ImageJ | NIH | – |
| SnapGene | Domatics | v7.0.2 |
| CellCyte Studio | Discover Echo | – |
| FlowJo | BD Biosciences | RRID:SCR_008520 |
| **Other** | | |
| Cytena CellCyteX | Discover Echo GmbH | – |
| Cytena Echo Revolve | Discover Echo GmbH | – |
| MaxCyte ATx system | MaxCyte | E-ATx |
| 12 mm glass coverslips | Electron Microscopy Sciences | Cat# 72230-01 |
| Bolt 4–12% Bis-Tris Plus gels | Invitrogen | Cat# NW04120 |
| Amersham Hybond P 0.2 μm PVDF membrane | GE Healthcare Life Sciences | Cat# 10600057 |
| Amersham Hybond-N+ nylon membrane | GE Healthcare Life Sciences | Cat# RPN303B |
| Minifold II Slot-Blot System | SRC | Cat# SRC072/0 |

(*Continued on next page*)

*Continued*

| REAGENT or RESOURCE | SOURCE | IDENTIFIER |
|---|---|---|
| 254 nm UV cross-linker | Stratagene | Cat# 400071-05 |
| Hybridization oven | Labnet | Cat# 05120804 |
| Nikon TiE Eclipse spinning disk confocal with FRAP | Nikon | – |
| G:Box chemi XX6 | Syngene | – |
| MACSQuant Analyzer 10 | Miltenyi Biotec | – |
| CellCyte X | Discover Echo | – |
| Biometra TRIO thermocycler | Analytik Jena | Cat# 846-4-070-723 |
| Bioruptor Pico sonicator | Diagenode | – |
| Bioruptor UCD-200 sonicator | Diagenode | – |
| MaxCyte ATx electroporation system | MaxCyte | Model ATx (E-ATx) |
| OC-25x3 electroporation cuvette | MaxCyte | Cat# SOC-25x3 |
| Nikon AXR Laser Scanning Confocal | Nikon | RRID: SCR_018302 |

## EXPERIMENTAL MODEL AND SUBJECT DETAILS

### Cell lines and cell culture

U2OS and SAOS2 are human cells derived from osteosarcoma of female patients, purchased from ATCC (HTB-96, HTB-85). U2OS cells were authenticated by STR profiling. VA13 are an *in vitro* immortalized clone of WI-38, a lung fibroblast line isolated from a female individual. VA13 cells were a generous gift from the Karlseder lab. HeLa ST and HeLa LT are subclones of HeLa cells, which were isolated from a female cervix adenocarcinoma. HeLa ST and HeLa LT are a generous gift from the Karlseder lab and were authenticated by STR profiling. Lenti-X 293T were derived from a transformed human embryonic kidney cell line and purchased from Takara Bio (#632180), and used for less than 5 passages. They were not further authenticated.

All cell lines were cultured in DMEM medium (Corning #10-013CV) supplemented with 10% Cosmic Calf Serum (Cytiva HyClone SH30087.04), 100 mg/mL Penicillin/Streptomycin L-Glutamine (Corning #30-009-CI), and 1X MEM Nonessential Amino Acids (Corning #25-025CI), maintained at 37°C in 3% $O_2$ and 7.5% $CO_2$, and tested for mycoplasma. The influence of sex as a variable was not investigated in this study.

Chemical compounds used include: Doxycycline (0.5 μM, TCI America, #D41165G), RO3306 (9 μM Millipore Sigma, #SML0569), colcemid (0.1 μg/mL, Gibco, #15212012), thymidine (2 mM, Millipore Sigma, #T9250), SUMOi (0.5 μM, Selleck Chemical, #S8697).

## METHOD DETAILS

### Plasmids and cell transductions and transfections

#### *Plasmids*

For TRF1-fusion plasmids, myc-TRF1, KRAB, and KDM4D fusion proteins were synthesized (gBlocks, IDT DNA) and cloned via In-Fusion (Takara Bio #638948) into a doxycycline-inducible lentiviral backbone with puromycin resistance (pLIX_403, a gift from David Root, Addgene plasmid #41395). For PML overexpression plasmids, PML-IV (Addgene plasmid #62804)[68] was cloned via In-Fusion (Takara Bio #638948) into a doxycycline-inducible lentiviral backbone with neomycin resistance (pCDNA3). HP1α gene sequences were a generous gift from the Blackburn lab (Addgene plasmid #17652). All subsequent modifications and cloning were achieved through PCR amplification and In-Fusion (Takara Bio) cloning. All plasmids were verified by restriction digest and full plasmid sequencing (QuintaraBio).

#### *Lentiviruses*

To produce lentivirus, 600,000 Lenti-X 293T cells (Takara Bio #632180) were seeded in a 6 well plate. After 24 h, cells were transfected with packaging plasmids (0.5 μg pCMV-VSV-G, 2.2 μg pCMV-dR8.9), 0.85 μg transfer plasmid, 7.35 μg of PEI (Polysciences Inc., #26008-5), and supplemented with 10 mM HEPES. Culture media was changed after 24 h with 2.5 mL complete DMEM supplemented with 10 mM HEPES. Culture media with virus was collected 48 h later and filtered through a 0.45μm PES Filter membrane (Whatman Uniflo, #9915–2504). Viral media and 8 μg/mL polybrene (Santa Cruz Biotechnology, #sc-134220) were added to cells for infection. Culture media was changed after 24 h with 2.5 mL complete DMEM. Cells were selected 24 h later with 1 μg/mL Puromycin (Thermo Scientific Chemicals, #J61278MC) until selection was complete of uninfected cells.

#### *siRNA transfection*

siRNA knockdowns were performed using Dharmacon ON-TARGETplus smartPOOL (Horizon Discovery). siRNA Non-targeting pool (UGGUUUACAUGUCGACUAA, UGGUUUACAUGUUGUGUGA, UGGUUUACAUGUUUUCUGA, UGGUUUACAUGUUUUCCUA); SP100 (GAAGUGAGCCUGUGAUCAA, AGGCAUAGAUCUAAAGUAA, UACCAGAGCCCAUGGAUUU, GAAGGGCACUCUAUA UAAG); ATRX (GAUGUUAGCUGGAUGUGUU, AGUCAUAGAUGCUAAGUUU, GCUUGAGGUUUCUGAAUUA, GUACAGGCGUUA

GCAUUAA); DAXX (CAGCCAAGCUCUAUGUCUA, GAGGUUAACAGGCGCAUUG GCAAAACAAAGGACGCAUA, GGAGUUGGAUC UCUCAGAA); SETDB1 (AAGAUGGGCUUUCAUGUUA, GAACUAAGACUUGGCACAA, GGGAUCAACCAGACAUAUA, GAGCGCA CCUGUUCGUAAG). HP1α knockdown was performed using a pool of two siRNAs targeting the 3′ untranslated region (3′UTR) (GUUGGAAUCUUACUAGUC and CUUCUGUAAAGUGAUAUC). 30 pmol (ATRX, HP1α, DAXX) or 60pmol (SETDB1) of siRNA (diluted in 150 μL of Opti-MEM I (Gibco, #31985-070) were mixed with 9 μL of Lipofectamine RNAiMAX Reagent (Thermo Fisher Scientific, #13778030) diluted in 150 μL of Opti-MEM I, incubated 5 min at room temperature (RT), and added to 140,000 cells diluted in 2 mL of complete media. The mix of cells, siRNAs and Lipofectamine were then seeded into 6-well plates and incubated for 72 h prior to collection.

#### *Poly(I:C) transfection*

Cells were induced with doxycycline for 48 h, then, while still maintained in doxycycline, ∼500,000 cells were seeded per well of a 6-well plate containing 4, 12 mm glass coverslips (Electron Microscopy Sciences Cat #72230-01). Transfection with Poly(I:C) was carried out 8 h later, allowing time for cells to settle and attach to coverslips. 1 mg/mL HMW Poly(I:C) (InvivoGen, #tlrl-pic) was added to 125 μL of Opti-MEM I (Gibco, #31985-070) and 2 μL of Lipofectamine 3000 ((Thermo Fisher Scientific, #L3000015) was added to 125 μL of Opti-MEM I. These were incubated 5 min at RT, mixed together, incubated for 20 min at RT, then added to experimental wells. 250 μL of Opti-MEM I was additionally added to control wells. Cells were treated with Poly(I:C) for 16 h, then fixed with 2% paraformaldehyde for 10 min at RT, and either directly used for IF-FISH or stored in PBS at 4°C.

### Western blots

Cells were collected by trypsinization, washed with cold PBS, and pellets were extracted with RIPA buffer (50 mM Tris-HCl pH 7.4, 150 mM NaCl, 1% NP-40, 0.5% sodium deoxycholate, 0.1% SDS) supplemented with 1X protease inhibitor (Roche_05892791001), and benzonase (1:100) (EMD Millipore Corp, #70746-3). Protein concentration was calculated using bicinchoninic acid (BCA) protein assay (Thermo Fisher Scientific, #23227). Twenty milligrams of protein were run on Bolt 4%–12% Bis-Tris Plus gels (Invitrogen, #NW04120) and transferred to a PVDF membrane (Amersham Hybond P 0.2 μm PVDF, GE Healthcare Life science, #10600057). Membranes were then blocked in 5% non-fat dry milk (NFDM) in PBS-Tween (PBS-T) for 30 min, incubated with primary antibodies diluted with 5% NFDM in PBS-T overnight at 4°C, washed three times in PBS-T, and incubated with HRP-conjugated secondary antibodies in 5% milk TBS-T for 45 min. The membranes were finally washed three times in PBS-T, and revealed with chemiluminescence (Prometheus ProSignal Dura, #20–301) using a G:Box chemi XX6 (Syngene).

#### *Antibodies used*

PML (Bethyl Laboratories Cat# A301-167A 1:200), SP100 (Abcam, #ab167605 dilution 1:1000), ATRX (Cell Signaling Technology, #E5X70 dilution 1:1000), SETDB1(Abcam, #ab107225 dilution 1:1000), DAXX (Cell Signaling Technology, #25C12 dilution 1:1000), HP1α (Abcam, #ab77256, dilution 1:1000), Myc-Tag (Cell Signaling Technology, #9B11 dilution 1:1000), Beta-Actin (Cell Signaling Technology #D6A8 1:1000), H3K9me3 (Abcam, #AB8898 1:3000), anti-Mouse HRP (Cell Signaling Technology, #7076S, dilution 1:5000) and anti-Rabbit-HRP (Cell Signaling Technology, #7074S, dilution 1:5000).

### Immunofluorescence and immunofluorescence-FISH

50,000 cells were seeded on 12 mm glass coverslips (Electron Microscopy Sciences Cat#72230-01) and treated according to each experiment. For immunofluorescence, cells were pre-extracted with cytoskeletal (CSK) buffer (10 mM Pipes, pH 7.0, 100 mM NaCl, 300 mM sucrose, and 3 mM $MgCl_2$) for 7 min on ice, washed with PBS and fixed with 2% paraformaldehyde in 1x PBS, washed with PBS, extracted with KCM buffer (100 mM KCl, 30 mM $CaCl_2$, 50 mM $MgCl_2$) for 10 min at room temperature (RT), and rinsed with PBS. Coverslips were then blocked with ABDIL buffer (20 mM Tris-HCl pH 7.5, 2% BSA, 0.2% Fish Gelatin, 150 mM NaCl, 0.1% Triton X-100, 0.1% Sodium Azide) for 20 min at 37°C, incubated 45 min at 37°C in a humidified chamber with primary antibodies diluted in ABDIL, washed in PBS-T, and incubated 1 h at room temperature with secondary antibodies diluted in ABDIL. Cells were washed with PBS and fixed with 2% paraformaldehyde. A final wash with 70% ethanol was performed to dry cells. Coverslips were then air dried and mounted onto slides with Fluoroshield with DAPI (Millipore Sigma F6057-20ML).

For FISH following IF, after incubation with secondary antibodies and PBS wash, cells were fixed with 2% paraformaldehyde. After three PBS washes, cells were dehydrated with sequential ethanol exposure (75%, 95% and 100%, 3 min each) and air dried on paper towel. Slides were inverted onto 5 μL 0.3 ng/μL of Alexa 488-OO-(CCCTAA)3 PNA probe (PNA Bio Inc., #F1001), diluted in 70% (v/v) deionized formamide (Millipore Sigma, #S4117); 0.25% (v/v) blocking reagent (Roche, #11096176001); 10 mM Tris-HCl pH 7.5; 4.1 mM $Na_2HPO_4$; 450 μM citric acid; 1.25 mM $MgCl_2$), denatured for 5 min at 84°C, and incubated in a humidity chamber at room temperature for 90 min. Coverslips were washed in a 24 well plate three times for 5 min with PNA Wash A (70% (v/v) formamide (Fisher, #F84-1); 10 mM Tris-HCl pH 7.5), then washed three times for 5 min with PNA Wash B (50 mM Tris-HCl pH 7.5; 150 mM NaCl; 0.08% Tween 20). After two washes with deionized water, coverslips were air dried on a paper towel and mounted with 5 μL Fluoroshield with DAPI (Millipore Sigma F6057-20ML). Cells were imaged using a Nikon TiE Eclipse spinning disk with FRAP, 60x objective. Images were analyzed in ImageJ and statistics were performed in GraphPad Prism.

#### *Antibodies used*

PML (Bethyl Laboratories Cat# A301-167A 1:200), PML (Santa Cruz Biotechnology, #sc-966 1:200), Myc-Tag (Cell Signaling Technology, #9B11 dilution 1:500), TRF2 (Novus, #NB110-57130 dilution 1:200), BLM (Bethyl Laboratories Cat# A300-110A dilution 1:1000), SP100 (Abcam, #ab167605 dilution 1:500), Alexa Fluor 568 goat anti-rabbit (Invitrogen, #A11036 1:400), Alexa Fluor

647 goat anti-mouse (Invitrogen, #A21236 1:400), Alexa Fluor 568 goat anti-mouse (Invitrogen, #A11031 1:400), Alexa Fluor 568 goat anti-Rabbit (Invitrogen, #A11008 1:400), Alexa Fluor 488 goat anti-mouse (Invitrogen, #A1101 1:400), Alexa Fluor 647 goat anti-mouse (Invitrogen, #A21236 1:400).

### *Subnuclear foci colocalization analysis and quantification*

Image stacks were acquired and processed in FIJI (ImageJ) using a custom macro. Maximum intensity projections were generated for each channel (z stack). For channels requiring foci detection and quantification background subtraction was performed using Gaussian blurring and image subtraction, followed by manual contrast adjustment to isolate subnuclear foci. Nuclei were then segmented from the DAPI channel by automated thresholding, mask conversion, and watershed. ROIs were manually curated to exclude artifacts as well as cells not exhibiting MYC signal, indicating a lack of induction. Within each ROI, foci were subsequently segmented using established thresholds, mask conversion, and watershed, and used for per nuclei foci quantifications. Colocalization events were defined as foci with >50% overlap and manually scored in merged, contrast-adjusted images.

### Flow cytometry for fusion construct expression

50,000 cells were doxycycline induced in a 12 well for 72 h. Cells were collected, washed with PBS, and resuspended in FACS buffer (PBS +2% Cosmic Calf Serum). Fluorescence was measured using a MACSQuant Analyzer 10 (Miltenyi), and cells were gated and quantified using FlowJo (BD Biosciences).

### C-circle assay

5 million cells were collected by trypsinization, pelleted by centrifugation and lysed in QCP lysis buffer (50 mM KCl, 10 mM Tris-HCl pH 8.5, 2 mM $MgCl_2$, 0.5% IGEPAL CA-630 detergent, 0.5% Tween 20) supplemented with protease (reconstituted 7.5 AU/7mL, 1:20 ratio used in QCP) (QIAGEN 19157). Phenol-chloroform extraction was performed to extract genomic DNA by mixing equal parts sample and Phenol/Chloroform/Isoamyl alcohol (25:24:1), stabilized, saturated with 100 mM Tris-EDTA to pH 8.0 (Acros Organics, #32711500) and centrifuged at 4°C. The aqueous layer was extracted, and mixed with equal parts chloroform (Fisher Chemical, #C574-1) and centrifuged at 4°C. The aqueous layer was collected and mixed with 2.5 parts ice-cold 100% ethanol (Decon Laboratories, Inc., #2701) and 0.1-part 3 M Sodium Acetate pH 5.2 (VWR, #0602-500G) and cooled at −20°C overnight. DNA pellets were collected by centrifugation at 4°C and the supernatant was removed. DNA was washed in 70% ethanol, centrifuged, dried and reconstituted in deionized water. 5μg of DNA was digested with 20 units of HinfI (NEB, #R0155L) and 20 units of RsaI (NEB, #R0167) in 1x Cutsmart buffer at 37°C for 2 h and purified with phenol-chloroform as described above. 10 ng of digested DNA was mixed with 8 mM Dithiothreitol, 1× Φ29 Buffer (New England Biolabs, #B0269S), 8 μg/mL recombinant albumin (New England Biolabs, #B9200S), 0.2% Tween 20, 2 mM each of dATP, dGTP, dTTP and dCTP (Qiagen Ref#201913), and 7.5 U of Φ29 DNA polymerase (NEB M0629L). Reactions were incubated at 30°C for 8 h followed by 70°C for 20 min and cooled to 12°C on a thermocycler (Biometra TRIO, analytik jena, #846-4-070-723). Samples were stored at −20°C or immediately used for slot blot hybridization.

### Slot blot hybridization

This protocol was adapted from Idilli et al., 2021. Each CCA reaction was blotted (Minifold II Slot-Blot System, SRC072/0) onto a positively charged nylon membrane (Amersham Hybond-N+, RPN303B), and wells were rinse with 400 μL 2X SSC. Samples were crosslinked for 1 min on each side of the membrane using a 254 nm UV cross-linker (Stratagene, 400071-05). The membrane was then placed on a nylon mesh in a hybridization tube with prehybridization buffer (5X SSC, 0.1% Sarkosyl (Sigma-Aldrich, #L7414-10ML), 0.04% SDS) and incubated in a rotating hybridization oven (Labnet, 05120804) at 65°C for 2 h. DIG-3′-end labeled probes were prepared using DIG Oligonucleotide 3′-End Labeling Kit, 2nd generation (Roche, #03353575910) following manufacturers protocols. Hybridization solution was prepared by combining prehybridization buffer with telomere (CCCTAA)4 DIG-3′-end or Alu 5′-GTAATCCCAGCACTTTGG DIG-3′-end labeled probe and incubated with the membrane for 18–20 h at 65°C. The membrane was then washed three times for 15 min with Wash Buffer 1 (2X SSC, 0.1% SDS) followed by a 20-min wash with 2× SSC. The membrane was placed in a heat sealable bag with 60 mL of blocking buffer (1% Blocking reagent (Roche, #11096176001), 0.1 M Maleic Acid (Cat#A14596.0B, 0.15 M NaCl)) for 30 min at RT, then incubated with Anti-Digoxigenin-AP, Fab fragments (Roche, #11093274910) (1:10,000 dilution) for 2 h at RT. After washing twice with Wash buffer 2 (0.1 M Maleic Acid, 0.3% Tween 20), the membrane was equilibrated in AP buffer (0.1 M Tris-HCl pH 9.5, 0.1 M NaCl). Chemiluminescence detection was carried out by diluting 50 μL of CDP-Star (Roche, #11759051001) in 5 mL of AP buffer and incubating with the membrane in a heat sealable bag for 30 min. Chemiluminescence was finally detected using a G:Box chemi XX6 (Syngene). Images were analyzed in ImageJ and statistics were performed in GraphPad Prism.

### Mitotic DNA synthesis

For mitotic DNA synthesis analysis, cells were doxycycline-induced induced for the entirety of this experiment (0.5 μg/mL). 72 h after the beginning of doxycycline induction, cells were thymidine blocked (2mM) for 24 h, washed, and incubated with CDK1 inhibitor (RO3306, Millipore Sigma, #SML0569, 9 μM) for 16 h. Cells were then washed for release into mitosis and incubated with EdU (10 μM) and colcemid (0.1 μg/mL) for 3 h. Cells and culture media was collected, centrifuged, and exposed to a hypotonic solution (75 mM KCl) at 37°C for 8 min, then fixed and washed 3 times with methanol:glacial acetic acid 3:1 (v/v). Metaphases were dropped onto glass slides placed over wet paper towels and dried overnight.

Metaphase slides were rehydrated in 1X PBS for 10 min, fixed with 3.7% formaldehyde in 1X PBS for 10 min, washed twice with 1X PBS, and digested for 10 min at 37°C with 1 mg/mL pepsin in citric acid pH 2 (Fisher Scientific, #A104-500). Slides were then washed twice with 1X PBS, fixed again in 3.7% formaldehyde in 1X PBS for 10 min, washed three more times in 1X PBS, dehydrated in ethanol baths (70%, 90%, 100%, 5 min each) and air dried. Slides were then overlayed with 40 μL of 0.3 ng/μL of Alexa 488-OO-(CCCTAA)3 PNA probe (PNA Bio Inc., #F1001), diluted in 70% (v/v) deionized formamide (Millipore Sigma, #S4117); 0.25% (v/v) blocking reagent (Roche, #11096176001); 10 mM Tris-HCl pH 7.5; 4.1 mM Na2HPO4; 450 μM citric acid; 1.25 mM $MgCl_2$, covered with a coverslip, denatured at 84°C for 3 min, and hybridized at room temperature overnight in a humidity chamber. Slides were then washed three times for 5 min in 70% (v/v) formamide, 10 mM Tris-HCl pH 7.5 and three times for 5 min in 50 mM Tris-HCl pH 7.5, 150 mM NaCl, 0.08% Tween 20. Slides were then dehydrated in successive ethanol baths and air dried. Finally, EdU was labeled with Click-iT EdU Cell Proliferation Kit for Imaging (Thermo Fisher Scientific, C10340) according to manufacturer's protocols and slides were mounted with Fluoroshield with DAPI (Millipore Sigma F6057-20ML). Images were analyzed in ImageJ and statistics were performed in GraphPad Prism.

### G2 EdU incorporation FISH

40,000 cells were seeded on 12 mm glass coverslips (Electron Microscopy Sciences Cat#72230-01) and doxycycline-induced induced for the entirety of this experiment (0.5 μg/mL). 72 h after the beginning of doxycycline induction, cells were thymidine blocked (2mM) for 24 h, washed, and incubated with CDK1 inhibitor (RO3306, Millipore Sigma, #SML0569, 9 μM) for 16 h. Cells were then washed for release and incubated with EdU (10 μM) and colcemid (0.1 μg/mL) for 1 h. EdU was labeled with Click-iT EdU Cell Proliferation Kit for Imaging (Thermo Fisher Scientific, C10340) according to manufacturer's protocols. Coverslips were stained for rabbit-*anti*-TRF2 (Novus, #NB110-57130 dilution 1:200) immunofluorescence as described above. Slides were mounted with Fluoroshield with DAPI (Millipore Sigma F6057-20ML). Cells were imaged using a Nikon TiE Eclipse spinning disk with FRAP, 60x objective. Images were analyzed in ImageJ and statistics were performed in GraphPad Prism.

### Chromatin immunoprecipitation

After three days of doxycycline induction (1 μM), 8 × 10 ^6 cells were harvested by trypsinization, resuspended in 10 mL of cold 1X PBS, and placed on ice. Cells were centrifuged and supernatant was discarded. Cells were fixed in in 1 mL of 1% formaldehyde in cold 1X PBS and incubated for 30 min at RT while rotating (for replicate N3, fixation was performed for 20 min). To quench the formaldehyde, 50 μL of 2.5 M glycine were added to the samples and incubated for 5 min at RT. The cells were then centrifuged, rinsed twice with 1 mL of 1X PBS on ice, and lysed in 300 μL of ChIP lysis buffer (1% SDS, 50 mM Tris-HCl pH 8, 10 mM EDTA pH 8) supplemented with protease inhibitor mix (Diagenode, #C12010011) and sonicated at 4°C using a 30-s "ON"/30-s "OFF" interval at high power for a total of 60 min with Diagenode Biorupter Pico (for replicate N3, sonication was performed using a Diagenode Biorupter UCD-200 for a total of 40 min, with 30-s ON/OFF cycles, and ice-cold water replacement every 10 min). The samples were centrifuged, and the supernatant was used immediately for immunoprecipitation.

Chromatin extracts were diluted to desired concentration with ice-cold ChIP dilution buffer supplemented with protease inhibitors. 1–10 μg of the desired antibody was added to chromatin extracts and incubated 4 h at 4°C on a rotating wheel. Protein A/G beads (Thermo Scientific, #88802) were then added (20–40 μL) and incubated overnight at 4°C on a rotating wheel.

Beads were washed on magnetic rack four times with 1 mL of cold ChIP wash buffer (0.1% SDS, 1% Triton X-100, 2 mM EDTA pH 8, 150 mM NaCl, 20 mM Tris-HCl pH 8), followed by one wash with 1 mL of cold ChIP final wash buffer (0.1% SDS, 1% Triton X-100, 2 mM EDTA pH8, 500 mM NaCl, 20 mM Tris-HCl pH 8). The immune complexes were eluted by adding 100 μL of ChIP elution buffer (1% SDS, 100 mM $NaHCO_3$) containing RNase A (40 μg/mL). For the input sample, 6 μL of 20% SDS,10 μL of 1 M $NaHCO_3$ were added, and supplemented with RNase A (40 μg/mL). Both the beads and input samples were incubated for 15 min at room temperature, then incubated for 1 h at 37°C. Cross-link reversal was performed by incubating the beads and input sample overnight at 65°C.

Samples were spun down briefly and incubated at RT for 30 min. DNA was then purified using a DNA purification kit (Qiagen, #28106) according to the manufacturer's instructions. The DNA was eluted in 50 μL of distilled water. DNA was denatured in 0.2 M NaOH at 100°C for 10 min, and the cooled-on ice. Samples were used for slot blot hybridization (as for C-circles, see above).

#### *Antibodies used*

H3 (Abcam, #AB1791, 3μg), H3K9me3 (Abcam, #AB8898, 5μg), HP1α (Abcam, #AB77256, 10 μg), IgG (Abcam, #AB37415, 5μg).

### Cell growth assay

Cells were seeded in a 24-well tissue culture plate and treated according to each experiment. Cells were maintained at 37°C in 3% O2 and 7.5% CO2. Live-cell imaging was performed using the CellCyte X (Discover Echo) positioned inside the incubator. Images were acquired every 6 h over the indicated time course. Confluency measurements were automatically calculated using the CellCyte Studio software, and data were exported for further analysis.

### Electroporation to generate KO cells

ATRX was knocked out in HeLa long telomere (HeLa LT) and HeLa short telomere (HeLa ST) cells, and heterozygous PML knockouts were generated in HeLa LT cells, using ribonucleoprotein (RNP) electroporation. Cas9 protein (IDT; 1081060) and synthetic sgRNAs targeting ATRX or PML (Synthego) were assembled into RNP complexes by mixing 2 μL of Cas9 (20 μM) with 5 μL of sgRNA (10 μM)

and 6.4 μL of nuclease-free water. The mixture was gently pipetted to ensure thorough mixing and incubated at room temperature for 20 min.

In parallel, 1.8 × 10 ^6 cells were collected, centrifuged at 500g for 3 min, and washed twice with 1X PBS. After the final wash, the cell pellet was resuspended in 25 μL of nucleofection buffer (MaxCyte; EPB-1) and combined with the pre-assembled RNP complex. The mixture was loaded into an OC-25x3 electroporation cuvette (MaxCyte; SOC-25x3) and electroporated using the "HeLa" setting on the MaxCyte ATx system (MaxCyte; E-ATx). Following electroporation, cells were transferred to 10 $cm^2$ plates containing 10 mL of pre-warmed supplemented DMEM and cultured under standard conditions. For HeLa LT and HeLa ST cells, heterozygous PML knockout and ATRX kockout clones were subsequently isolated by standard clonal expansion.

Telomere restriction fragment assay:

TRF was performed as described in Wu et al.[70]

## QUANTIFICATIONS AND STATISTICAL ANALYSES

Data analyses and statistics were performed using Prism 10 as indicated for each figure in the figure legend.